

DRAFT VERSION NOVEMBER 17, 2021

Typeset using L^AT_EX preprint style in AASTeX62

Overview of the DESI Legacy Imaging Surveys

ARJUN DEY,¹ DAVID J. SCHLEGEL,² DUSTIN LANG,^{3,4,5} ROBERT BLUM,¹ KAYLAN BURLEIGH,²
 XIAOHUI FAN,⁶ JOSEPH R. FINDLAY,⁷ DOUG FINKBEINER,⁸ DAVID HERRERA,¹ STÉPHANIE JUNEAU,¹
 MARTIN LANDRIAU,² MICHAEL LEVI,² IAN MCGREER,⁶ AARON MEISNER,² ADAM D. MYERS,⁷
 JOHN MOUSTAKAS,⁹ PETER NUGENT,² ANNA PATEJ,⁶ EDWARD F. SCHLAFLY,²
 ALISTAIR R. WALKER,¹⁰ FRANCISCO VALDES,¹ BENJAMIN A. WEAVER,¹ CHRISTOPHE YÈCHE,¹¹
 HU ZOU,¹² XU ZHOU,¹² BEHZAD ABARESHI,¹ T. M. C. ABBOTT,¹⁰ BELA ABOLFATHI,¹³
 C. AGUILERA,¹⁰ LORI ALLEN,¹ A. ALVAREZ,¹⁰ JAMES ANNIS,¹⁴ MARIE AUBERT,¹⁵ ERIC F. BELL,¹⁶
 SEGEV Y. BENZVI,¹⁷ RICHARD M. BIELBY,¹⁸ ADAM S. BOLTON,¹ CÉSAR BRICEÑO,¹⁰
 ELIZABETH J. BUCKLEY-GEER,¹⁴ KAREN BUTLER,¹ ANNALISA CALAMIDA,¹⁹
 RAYMOND G. CARLBERG,⁴ PAUL CARTER,²⁰ RICARD CASAS,^{21,22} FRANCISCO J. CASTANDER,^{21,22}
 YUMI CHOI,⁶ JOHAN COMPARAT,²³ ELENA CUKANOVAITE,²⁴ TIMOTHÉE DELUBAC,²⁵
 KAITLIN DeVRIES,²⁶ SHARMILA DEY,²⁷ GOVINDA DHUNGANA,²⁸ MARK DICKINSON,¹ ZHEJIE DING,²⁹
 JOHN B. DONALDSON,¹ YUTONG DUAN,³⁰ CHRISTOPHER J. DUCKWORTH,³¹ SARAH EFTEKHARZADEH,⁷
 DANIEL J. EISENSTEIN,⁸ THOMAS ETourneau,¹¹ PARKER A. FAGRELIUS,³² JAY FARIHI,³³
 MIKE FITZPATRICK,¹ ANDREU FONT-RIBERA,³³ LEAH FULMER,¹ BORIS T. GÄNSICKE,²⁴
 ENRIQUE GAZTANAGA,^{21,22} KOSHY GEORGE,³⁴ DAVID W. GERDES,³⁵
 SATYA GONTCHO A GONTCHO,³³ GREGORY GREEN,⁸ JULIEN GUY,² DIANE HARMER,¹
 M. HERNANDEZ,¹⁰ KLAUS HONSCHIED,³⁶ LIJUAN (WENDY) HUANG,¹ DAVID JAMES,⁸
 BUELL T. JANNUZI,⁶ LINHUA JIANG,³⁷ RICHARD JOYCE,¹ ARMIN KARCHER,² SONIA KARKAR,³⁸
 ROBERT KEHOE,²⁸ JEAN-PAUL, KNEIB,^{25,39} ANDREA KUETER-YOUNG,⁴⁰ TING-WEN LAN,⁴¹
 TOD LAUER,¹ LAURENT LE GUILLOU,³⁸ AUGUSTE LE VAN SUU,⁴² JAE HYEON LEE,⁴³
 MICHAEL LESSER,⁶ TING S. LI,¹⁴ JUSTIN L. MANN,⁴⁴ BOB MARSHALL,¹ C. E. MARTÍNEZ-VÁZQUEZ,¹⁰
 PAUL MARTINI,⁴⁵ HÉLION DU MAS DES BOURBOUX,⁴⁶ SEAN MCMANUS,¹ BRICE MÉNARD,⁴⁷
 NIGEL METCALFE,¹⁸ ANDREA MUÑOZ-GUTIÉRREZ,⁴⁸ JOAN NAJITA,¹ KEVIN NAPIER,⁹
 GAUTHAM NARAYAN,¹⁹ JEFFREY A. NEWMAN,⁴⁹ JUNDAN NIE,¹² BRIAN NORD,^{14,50}
 DARA J. NORMAN,¹ KNUT A.G. OLSEN,¹ ANTHONY PAAT,¹ NATHALIE PALANQUE-DELABROUILLE,¹¹
 XIYAN PENG,¹² CLAIRE L. POPPETT,⁵¹ MEGAN R. POREMBA,⁹ ABHISHEK PRAKASH,⁵²
 DAVID RABINOWITZ,⁵³ ANAND RAICHOOR,²⁵ MEHDI REZAIE,²⁹ A. N. ROBERTSON,¹ NATALIE A. ROE,²
 ASHLEY J. ROSS,⁵⁴ NICHOLAS P. ROSS,⁵⁵ GREGORY RUDNICK,⁴⁴ SASHA SAFONOVA,⁵⁶ ABHIJIT SAHA,¹
 F. JAVIER SÁNCHEZ,¹³ HEIDI SCHWEIKER,¹ ADAM SCOTT,¹ HEE-JONG SEO,⁵⁷ HUANYUAN SHAN,⁵⁸
 DAVID R. SILVA,¹ CHRISTIAN SOTO,¹ DAVID SPRAYBERRY,¹ RYAN STATEN,²⁸ COLEY M. STILLMAN,⁹
 ROBERT J. STUPAK,¹ DAVID L. SUMMERS,¹ SUK SIEN TIE,⁴⁵ H. TIRADO,¹⁰
 MARIANA VARGAS-MAGAÑA,⁴⁸ A. KATHERINA VIVAS,¹⁰ RISA H. WECHSLER,^{59,60} DOUG WILLIAMS,¹
 JINYI YANG,⁶ QIAN YANG,⁶¹ TOLGA YAPICI,¹⁷ DENNIS ZARITSKY,⁶ A. ZENTENO,¹⁰ KAI ZHANG,²
 TIANMENG ZHANG,¹² RONGPU ZHOU,⁴⁹ AND ZHIMIN ZHOU¹²

¹National Optical Astronomy Observatory, 950 N. Cherry Ave., Tucson, AZ 85719

²Lawrence Berkeley National Laboratory, 1 Cyclotron Rd., Berkeley, CA 94720

³Dunlap Institute, University of Toronto, Toronto, ON M5S 3H4, Canada

⁴Department of Astronomy & Astrophysics, University of Toronto, Toronto, ON M5S 3H4, Canada

⁵Perimeter Institute for Theoretical Physics, Waterloo, ON N2L 2Y5, Canada

⁶Steward Observatory, University of Arizona, 933 N. Cherry Ave., Tucson, AZ 85721

⁷Department of Physics & Astronomy, University of Wyoming, 1000 E. University, Dept 3905, Laramie, WY 8207

- ⁸*Harvard-Smithsonian Center for Astrophysics, 60 Garden St., Cambridge, MA 02138*
- ⁹*Department of Physics and Astronomy, Siena College, 515 Loudon Rd., Loudonville, NY 12211*
- ¹⁰*Cerro Tololo Inter-American Observatory, National Optical Astronomy Observatory, Casilla 603, La Serena, Chile*
- ¹¹*IRFU, CEA, Université Paris-Saclay, F-91191 Gif-sur-Yvette, France*
- ¹²*Key Laboratory of Optical Astronomy, National Astronomical Observatories, Chinese Academy of Sciences, Beijing 100012, China*
- ¹³*Department of Physics and Astronomy, University of California, Irvine, Irvine, CA 92697*
- ¹⁴*Fermi National Accelerator Laboratory, P.O. Box 500, Batavia, IL 60510*
- ¹⁵*Aix Marseille Univ, CNRS/IN2P3, CPPM, Marseille, France*
- ¹⁶*Department of Astronomy, University of Michigan, 1085 S. University Ave., Ann Arbor, MI, 48109*
- ¹⁷*Department of Physics and Astronomy, University of Rochester, 500 Wilson Blvd., Rochester, NY 14627*
- ¹⁸*Centre for Extragalactic Astronomy, Durham University, South Rd., Durham, DH1 3LE, UK*
- ¹⁹*Space Telescope Science Institute, 3700 San Martin Dr., Baltimore, MD 21218*
- ²⁰*Institute of Cosmology & Gravitation, University of Portsmouth, Dennis Sciama Building, Portsmouth PO1 3FX, UK*
- ²¹*Institute of Space Sciences (ICE, CSIC), Campus UAB, Carrer de Can Magrans, s/n, 08193 Barcelona, Spain*
- ²²*Institut d'Estudis Espacials de Catalunya (IEEC), 08193 Barcelona, Spain*
- ²³*Max-Planck Institut für extraterrestrische Physik, Postfach 1312, D-85741 Garching bei München, Germany*
- ²⁴*Department of Physics, University of Warwick, Coventry CV4 7AL, UK*
- ²⁵*Institute of Physics, Laboratory of Astrophysics, Ecole Polytechnique Fédérale de Lausanne (EPFL), Observatoire de Sauverny, 1290 Versoix, Switzerland*
- ²⁶*Bentley School, 1000 Upper Happy Valley Rd., Lafayette, CA 94549*
- ²⁷*University High School, 421 N Arcadia Ave., Tucson, AZ 85711*
- ²⁸*Department of Physics, Southern Methodist University, 3215 Daniel Ave., Dallas, TX, 75205*
- ²⁹*Department of Physics and Astronomy, Ohio University, Clippinger Labs, Athens, OH 45701*
- ³⁰*Boston University Physics Department, 590 Commonwealth Ave., Boston, MA 02215*
- ³¹*School of Physics and Astronomy, University of St Andrews, North Haugh, St Andrews KY16 9SS, UK*
- ³²*Department of Physics, University of California, Berkeley, Berkeley, CA 94720*
- ³³*Department of Physics and Astronomy, University College London, London WC1E 6BT, UK*
- ³⁴*Indian Institute of Astrophysics, Koramangala II Block, Bangalore, India*
- ³⁵*Department of Physics, University of Michigan, Ann Arbor, MI 48109*
- ³⁶*Department of Physics, Ohio State University, 191 W. Woodruff Ave., Columbus, OH 43210*
- ³⁷*Kavli Institute for Astronomy and Astrophysics, Peking University, Beijing 100871, China*
- ³⁸*Sorbonne Université, Université Paris-Diderot, CNRS-IN2P3, Laboratoire de Physique Nucléaire et de Hautes Energies, LPNHE, F-75005 Paris, France*
- ³⁹*Aix Marseille Université, CNRS, LAM (Laboratoire d'Astrophysique de Marseille) UMR 7326, 13388, Marseille, France*
- ⁴⁰*Department of Physics & Astronomy, Rutgers University, 136 Frelinghuysen Rd., Piscataway, NJ 08854-8019*
- ⁴¹*Kavli IPMU, The University of Tokyo (WPI), Kashiwa 277-8583, Japan*
- ⁴²*Aix Marseille University, CNRS, Observatoire Haute Provence, 04870 St-Michel-l'Observatoire, France*
- ⁴³*Physics Department, Harvard University, Cambridge, MA 02138, USA*
- ⁴⁴*Department of Physics and Astronomy, University of Kansas, 1251 Wescoe Hall Dr., Room 1082, Lawrence, KS 66045*
- ⁴⁵*Department of Astronomy and Center for Cosmology and Astroparticle Physics, The Ohio State University, Columbus, OH 43210*
- ⁴⁶*Department of Physics and Astronomy, University of Utah, 115 S. 1400 E., Salt Lake City, UT 84112*
- ⁴⁷*Johns Hopkins University, Department of Physics & Astronomy, 3400 N. Charles St., Baltimore, MD 21218*

⁴⁸*Instituto de Física, Universidad Nacional Autónoma de México, A.P. 20-364, 04510 Ciudad de México, México*

⁴⁹*Department of Physics and Astronomy and PITT PACC, University of Pittsburgh, 3941 O'Hara St., Pittsburgh, PA 15260*

⁵⁰*Kavli Institute for Cosmological Physics, University of Chicago, Chicago, IL 60637*

⁵¹*Space Sciences Lab, UC Berkeley, Berkeley, CA 94720*

⁵²*Infrared Processing and Analysis Center (IPAC), California Institute of Technology, 1200 E. California Blvd., Pasadena, CA 91125*

⁵³*Yale University Physics Department, P.O. Box 2018120, New Haven, CT 06520-8120*

⁵⁴*Center for Cosmology and AstroParticle Physics, The Ohio State University, Columbus, OH 43210*

⁵⁵*Institute for Astronomy, University of Edinburgh, Royal Observatory, Blackford Hill, Edinburgh EH9 3HJ, UK*

⁵⁶*Lawrence Livermore National Laboratory, 7000 East Ave., Livermore, CA 94550*

⁵⁷*Department of Physics and Astronomy, Ohio University, Clippinger Labs, Athens, OH 45701, USA*

⁵⁸*Argelander-Institut für Astronomie, Auf dem Hügel 71, 53121 Bonn, Germany*

⁵⁹*Kavli Institute for Particle Astrophysics and Cosmology and Department of Physics, Stanford University, Stanford, CA 94305, USA*

⁶⁰*Department of Particle Physics and Astrophysics, SLAC National Accelerator Laboratory, Stanford, CA 94305, USA*

⁶¹*Department of Astronomy, School of Physics, Peking University, Beijing 100871, China*

Submitted to Astronomical Journal (AJ)

Abstract

The DESI Legacy Imaging Surveys are a combination of three public projects (the Dark Energy Camera Legacy Survey, the Beijing-Arizona Sky Survey, and the Mayall z -band Legacy Survey) that will jointly image $\approx 14,000$ deg² of the extragalactic sky visible from the northern hemisphere in three optical bands (g , r , and z) using telescopes at the Kitt Peak National Observatory and the Cerro Tololo Inter-American Observatory. The combined survey footprint is split into two contiguous areas by the Galactic plane. The optical imaging is conducted using a unique strategy of dynamic observing that results in a survey of nearly uniform depth. In addition to calibrated images, the project is delivering an inference-based catalog which includes photometry from the grz optical bands and from four mid-infrared bands (at $3.4\mu\text{m}$, $4.6\mu\text{m}$, $12\mu\text{m}$ and $22\mu\text{m}$) observed by the *Wide-field Infrared Survey Explorer* (*WISE*) satellite during its full operational lifetime. The project plans two public data releases each year. All the software used to generate the catalogs is also released with the data. This paper provides an overview of the Legacy Surveys project.

Keywords: surveys – catalogs

1. INTRODUCTION

Explorations of the universe begin with images. In the last few decades, systematic surveys of the sky across the electromagnetic spectrum have revolutionized the ways in which we study physical processes in known astronomical sources, identify new astrophysical sources and phenomena, and map our environs (e.g., see Djorgovski et al. 2013, for an excellent summary). The amazing bounty of wide-field imaging surveys at optical wavelengths has been recently, and spectacularly, demonstrated by the Sloan Digital Sky Survey (SDSS; Abazajian et al. 2009), Pan-STARRS1 (PS1; Chambers

et al. 2016) and the Dark Energy Survey (The Dark Energy Survey Collaboration 2005), all of which continue to advance our knowledge of the universe in multiple fields of astrophysics (e.g., Dark Energy Survey Collaboration et al. 2016).

In this paper we describe the DESI Legacy Imaging Surveys (hereafter The Legacy Surveys) aimed at mapping 14,000 deg² of the extragalactic sky in three optical bands (g , r and z). The very wide areal coverage and the need to finish the survey in less than three years necessitated the use of three different telescope platforms: the Blanco telescope at the Cerro Tololo Inter-American Observatory; the Mayall Telescope at the Kitt Peak National Observatory; and the University of Arizona Steward Observatory 2.3m (90inch) Bart Bok Telescope at Kitt Peak National Observatory. In addition, the Legacy Surveys source catalogs incorporate mid-infrared photometry for all optically-detected sources from new image stacks of data from the *Wide-field Infrared Survey Explorer* satellite (Wright et al. 2010).

2. MOTIVATION FOR A NEW WIDE-FIELD IMAGING SURVEY

2.1. *Imaging for the Dark Energy Spectroscopic Instrument Surveys*

The Legacy Surveys are motivated by the need to provide targets for the Dark Energy Spectroscopic Instrument (DESI) survey. DESI is an international project that is constructing a 5000-fiber multi-object spectrograph for the Mayall 4m telescope at the Kitt Peak National Observatory (DESI Collaboration et al. 2016b). Over a five-year period (2019–2024), DESI will measure the redshifts of 35 million galaxies and quasars, including $\sim 700,000$ QSOs at $z > 2.1$ ¹ suitable for probing the structure of the intergalactic medium at high redshift (DESI Collaboration et al. 2016a). The DESI Key Project will use these maps of the large scale matter distribution traced by galaxies and the Lyman- α forest to measure the expansion history of the universe over the past 10 billion years. The goal is to provide sub-percent accuracy constraints on the equation of state of dark energy and its time evolution (cf. Alam et al. 2017). The DESI project will also provide precise constraints on the growth of structure in the universe by using measurements of redshift-space distortions (e.g., Guzzo et al. 2008; Blake et al. 2011; Pezzotta et al. 2017). In order to reach percent-level precision on the cosmological parameters, the DESI survey requires spatially dense samples of galaxy and QSO tracers across very large areas of the sky ($>10,000$ deg²). The SDSS and PS1 surveys are both too shallow to reliably select the DESI targets, and the SDSS footprint is too small. The DES survey reaches adequate depth, but covers only 5000 deg² mainly in regions too far south to be reached from Kitt Peak. These considerations motivated the Legacy Surveys, which are deeper than SDSS and PS1 and cover a much larger area than DES in the northern sky. Imaging for the Legacy Surveys is on track to be completed prior to the start of the DESI spectroscopic survey in 2019. The detailed requirements placed by the DESI target selection on the imaging surveys are described in more detail in an Appendix to this paper (see § A1).

2.2. *Complementing Existing Spectroscopy*

Beyond the primary goal of providing DESI targets, the imaging survey described in this paper has more wide-ranging astrophysical motivations. The Sloan Digital Sky Survey (SDSS; e.g., Abazajian et al. 2009) project has overwhelmingly demonstrated the power of combining wide-field imaging and spectroscopic surveys within the same footprint. The SDSS-I,II,III/BOSS surveys contain ~ 2.8

¹ We shall use the terms “quasar” and “QSO” interchangeably throughout this paper.

million spectra, including 300,000 unique stars, 700,000 galaxies at $z < 0.2$, 500,000 galaxies at $0.2 < z < 0.5$, 1 million galaxies at $z > 0.5$, 100,000 QSOs at $z < 2$, and 200,000 QSOs at $z > 2$.² The median extragalactic redshift of these samples is already $z_{\text{med}} \approx 0.5$, and SDSS-IV/eBOSS (Dawson et al. 2016, 2014–2020) is currently adding another 600,000 galaxies at $0.6 < z < 1$ (Prakash et al. 2016; Raichoor et al. 2017) and 500,000 new QSOs at $z > 0.9$ (Myers et al. 2015). Most of these data are already available publicly.

While most SDSS-I spectra targeted nearby galaxies ($r < 17.77$; i.e., 4–5 magnitudes brighter than the imaging detection limit), BOSS (SDSS-III) targeted much fainter sources (galaxies to $i = 19.9$ and QSOs to $g = 22$), near the limits of the original SDSS imaging (Dawson et al. 2013); eBOSS (SDSS-IV) goes even fainter. While adequate for the study of large-scale structure, the full science impact of these data is limited by the depth and quality of the existing imaging. The bulk of existing spectroscopic redshifts are in the northern sky and have poor overlap with most deep, wide-field imaging surveys (see Figure 1). The SDSS imaging data (which provided the spectroscopic targets) do not provide precise photometry, well-resolved size measurements, detailed morphologies, or environmental measures for the bulk of the faint galaxies targeted by the existing spectroscopy.

The Legacy Surveys will greatly remedy this situation by imaging the entire BOSS footprint to magnitudes suitable for the study of the $z > 0.5$ universe (see Figure 1). Imaging 1.5–2 magnitudes fainter in three optical bands, should increase the number of $z > 0.5$ ($z > 1$) galaxies by a factor of ~ 30 (~ 600) over SDSS (Fig. 3b). Measuring $g - r$ vs. $r - z$ colors cleanly isolates $z > 0.5$ galaxies. Optical photometry coupled with the *WISE* mid-infrared photometry can be used to measure stellar masses and AGN activity for such galaxies (see, e.g., § 3 of DESI Collaboration et al. 2016a, and references therein). The improved image quality ($\text{FWHM} \approx 1''$) and depth of the Legacy Surveys can be used to resolve morphologies and structural parameters for all SDSS spectroscopic galaxies.

Spectroscopy complements deep imaging; it provides: robust redshifts; a crisp 3-d view of large-scale structure; dynamical information through velocity dispersions; spectral diagnostics of stellar populations, star formation rates, and nuclear activity; and probes of the intergalactic medium through absorption line studies. The combination enables numerous astrophysical studies. For example:

- *The Evolution of Galaxy Clusters:* While SDSS has obtained redshifts of 1.5 million massive galaxies, often the central, brightest galaxies in groups and clusters, current imaging often cannot detect their satellites. The Legacy Surveys will significantly improve stellar mass models for these galaxies and enable a sensitive search for faint cluster members. Extrapolating from the SDSS Stripe 82 imaging (Rykoff et al. 2014, 2016), we expect to identify $\sim 75,000$ clusters, nearly all of which will have spectroscopic redshifts available from SDSS. Spectroscopy provides three key benefits not available to photometric-only surveys: 1) calibration of cluster masses by stacked velocity dispersion measurements (e.g., Becker et al. 2007); 2) tests of general relativity by the comparison of the velocity field around clusters to the weak lensing shear mass profile (e.g., Lam et al. 2012; Zu et al. 2014); and 3) calibration of cluster masses by detecting the weak-lensing magnification of the luminosity function of background galaxies and quasars (Coupon et al. 2013, 2015). Magnification-based methods have systematic uncertainties that are completely independent from the shape and photometric redshift systematics expected

² <http://sdss3.org>

to dominate the error budget of imaging-only surveys like DES or LSST, thereby enabling a critical consistency test with these surveys.

- *Galaxy Halos Through Cosmic Time:* The contents (and shapes) of galaxy dark matter halos can be revealed from the cross-correlation of spectroscopic and imaging maps (Eisenstein et al. 2005; Tal et al. 2013) and from galaxy-galaxy weak lensing (e.g., Mandelbaum et al. 2016). These methodologies benefit substantially from deeper imaging, the precision scaling as $\sqrt{N_{gal}}$. Higher precision is crucial: variations in clustering as a function of galaxy properties are often only of order 10%, so distinguishing between models requires percent-level clustering measurements. The $z \sim 23$ depth of the Legacy Surveys (e.g., $\sim 0.5L^*$ at $z=0.7$) will increase the samples available to these methodologies by factors of 30 or more. Cross-correlation studies use angular correlations to tie deep photometric catalogs to overlapping spectroscopic maps, measuring the mean environments and clustering of galaxies and AGN with great accuracy. SDSS has provided high-precision results at lower redshift using these techniques, e.g., measuring the mean environment of galaxies as a function of luminosity, color, and scale (Hogg et al. 2003; Eisenstein et al. 2005; Masjedi et al. 2006; Jiang et al. 2012) and interpreting this to constrain halo populations and merger rates (Zheng et al. 2009; Watson et al. 2012). The Legacy Surveys will extend this to far larger ($>10\text{--}100\times$) spectroscopic and photometric samples at high redshift, measuring the satellite distributions around central galaxies as a function of redshift, luminosity, stellar mass, color, major axis orientation, velocity dispersion, [O II] emission line equivalent width, etc. Cross-correlation also enables more robust clustering measurements around rare spectroscopic populations, and the ability to calibrate galaxy redshift distributions from imaging data (Newman 2008; Myers et al. 2009; Ménard et al. 2013; Schmidt et al. 2013).
- *The Evolution of Halo Gas:* SDSS spectra have already yielded $>50,000$ MgII absorption line systems at $0.4 < z < 2.5$ toward background QSOs (Zhu & Ménard 2013), and eBOSS will increase the number of sightlines to nearly a million. By cross-correlating 2,000 absorbers at $z \sim 0.5$ with SDSS photometric galaxies, Lan et al. (2014) extracted new relations between galaxy properties and their surrounding gas (e.g., their Fig. 2a). The Legacy Surveys will dramatically improve this type of analysis by extending its reach from $z \sim 0.5$ to $z \sim 2$, sampling the full range of $\sim 100,000$ identified absorbers. This will map the cosmic evolution of halo gas as a function of redshift, making it possible to understand its dependence on galaxy type, orientation, luminosity, star-formation rate, environment, etc.
- *The Halo of the Milky Way:* The SDSS, PS1 and DES imaging surveys have revolutionized the study of the Milky Way, finding numerous stellar halo streams (e.g., Newberg et al. 2002; Yanny et al. 2003; Grillmair 2009; Bernard et al. 2016; Shipp et al. 2018) and dwarf galaxies (Willman et al. 2005; Laevens et al. 2014; Drlica-Wagner et al. 2015; Bechtol et al. 2015). The Legacy Surveys will map at least twice as far out into the Galactic halo over $14,000 \text{ deg}^2$, increasing the volume of the MW explored by a factor of ~ 5 relative to SDSS+Pan-STARRS. This will enable tests of predictions that stellar halo substructure dramatically increases with distance (Bell et al. 2008; Helmi et al. 2011). Our photometric parallax-based maps will extend to $\sim 40 \text{ kpc}$ using main sequence stars (Ivezić et al. 2008; Jurić et al. 2008), $\sim 80 \text{ kpc}$ using *gr*-selected main sequence turnoff stars (Bell et al. 2008), and $\sim 150 \text{ kpc}$ using *ugr*-identified Blue Horizontal Branch (BHB) stars where *u*-band is available (Ruhland et al. 2011). The deeper

data on known streams (Odenkirchen et al. 2003; Carballo-Bello et al. 2018) will be used to test for the presence of “missing satellites” via their signatures in these streams (Carlberg 2009; Yoon et al. 2011). Imaging from the Legacy Surveys should be sufficient to discover 8–20 new dwarf galaxies. Each dwarf galaxy discovery immediately adds years of Fermi integration to the search for dark matter detection via gamma rays (Albert et al. 2017). Finally, given the 10-year time baseline between imaging from SDSS and the Legacy Surveys, proper motions should be measured to accuracies of a few milliarcsec per year for stars 2 mag fainter than the Gaia limits.

2.3. Photometry from the *WISE* Satellite

The Legacy Surveys will greatly enhance in the utility of the mid-IR imaging data from the *WISE* satellite by providing deep template *grz* optical images for matched photometry using *The Tractor* package (Lang et al. 2016a, see § 8). By optimally matching *WISE* to deep optical imaging, one can partially deblend the images of confused *WISE* sources and improve the signal-to-noise ratio of their mid-infrared photometry and color measurements. Using SDSS *r*-band templates already shows substantial improvement, but the deeper Legacy Surveys images will allow extraction of fainter, higher redshift sources. The extended *WISE* mission will more than quadruple the exposure time of the original *WISE* all-sky survey (cf. the AllWISE catalog) in the 3.4 and 4.6 μm bands by the end of 2018 and provide multiple epochs for identification of mid-infrared variable sources. The Legacy Surveys will provide matched *WISE* mid-infrared photometry for hundreds of millions of optical sources. Properly matched optical-to-mid-IR photometry will allow more robust estimation of stellar masses and improved photometric redshifts for extragalactic objects. Such photometry will also facilitate high-fidelity selection of massive galaxies to $z \sim 1.5$ –2, and the selection of nearly all optically detected quasars.

3. FOOTPRINT

The footprint of the Legacy Surveys is designed to correspond to the DESI Survey footprint, which is defined to be the extragalactic sky above a Galactic latitude of $b = 15^\circ$ that can be observed spectroscopically from Kitt Peak (i.e., at declination $\delta > -20^\circ$). These selections result in an $\approx 14,000 \text{ deg}^2$ area, which contains two contiguous regions, one in the North Galactic Cap (NGC) covering 9900 deg^2 and one in the South Galactic Cap (SGC) covering 4400 deg^2 .

The basic criteria described result in a larger area in the NGC (A semester) relative to the SGC (B semester). However, we also need to conduct a uniform, wide-area extragalactic survey with fields that can be scheduled throughout the year, minimizing observations at high airmass (at low or high declinations) and in regions of high Galactic extinction or high stellar density. To minimize scheduling issues for DESI, the NGC portion of the footprint is trimmed to declination $\delta > -8.2^\circ$ and the SGC area extends southward to $\delta \approx -13.3^\circ$ in regions not covered by the Dark Energy Survey (DES; The Dark Energy Survey Collaboration 2005), and to $\delta \approx -18.4^\circ$ in the region covered by DES. These choices were informed by realistic simulations of the DESI survey including a dynamic observing model similar to that described in § 6.2.

Since the primary motivation is an extragalactic cosmological survey, additional cuts are imposed to remove those parts of the sky with the largest stellar density. For the survey regions closest to the Galactic center (i.e., $-90^\circ < l < +90^\circ$), only regions with Galactic latitude $|b| > 18^\circ$ are selected;

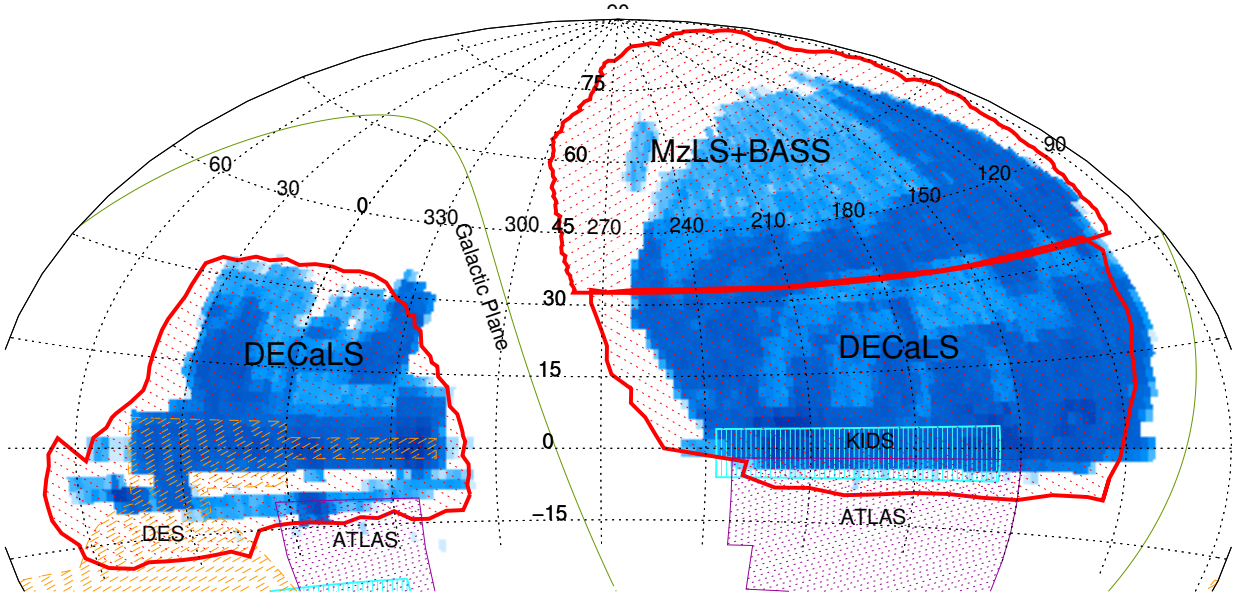


Figure 1. The footprints of the optical imaging surveys contributing to DESI imaging, demarcated by the thick red outlines, are shown here in an equal-area Aitoff projection in equatorial coordinates. The region covered by the BASS and MzLS surveys is almost entirely in the North Galactic Cap (NGC) at declinations $\delta \geq +32^\circ$, and DECaLS covers the entire South Galactic Cap and the $\delta \leq +34$ regions in the NGC. The regions covered by existing wide-area spectroscopic redshift surveys (SDSS, BOSS and 2dF) are shown in the blue greyscale in the map above, where the darker colors represent a higher density of spectroscopic redshifts. The Legacy Surveys provide deeper imaging and can leverage the existing spectroscopy in these regions, unlike most other existing or ongoing deep imaging surveys (e.g., DES, ATLAS, KIDS, etc.; The Dark Energy Survey Collaboration 2005; Shanks et al. 2015; de Jong et al. 2015).

in the Galactic anti-center, a less stringent criterion of $|b| > 14^\circ$ is imposed, allowing the survey to extend a bit closer to the Galactic plane.

Finally, the selected footprint is modified to both avoid small holes within the survey and to avoid largely disconnected regions. An “orphaned” area of 600 deg^2 in the northern part of the SGC has therefore been excluded from the DESI footprint.

The final footprint is shown in Figure 1. The DESI spectroscopic survey is expected to observe most or all this footprint, dependent upon the level of completion of the Legacy Surveys.

4. THE THREE SURVEYS

The four target classes that will be used as cosmological tracers by DESI can be selected using a combination of optical imaging data in the g , r , and z bands and mid-infrared imaging in the $3.4 \mu\text{m}$ and $4.6 \mu\text{m}$ *WISE* bands (see § A for further details). DESI requires that the Legacy Surveys deliver 5σ detections of a “fiducial” $g=24.0$, $r=23.4$ and $z=22.5$ AB mag galaxy with an exponential light profile of half-light radius $r_{\text{half}} = 0.45 \text{ arcsec}$. DESI also requires the depth (and the resulting target selection) to be as uniform as possible across the survey footprint. Ideally, a cosmological survey would use the same imaging data to select all science and calibration targets. However, the ambitious footprint coupled with the short timeline for DESI and lack of very-wide-field imaging capabilities in the northern hemisphere necessitated using multiple platforms to cover the footprint.

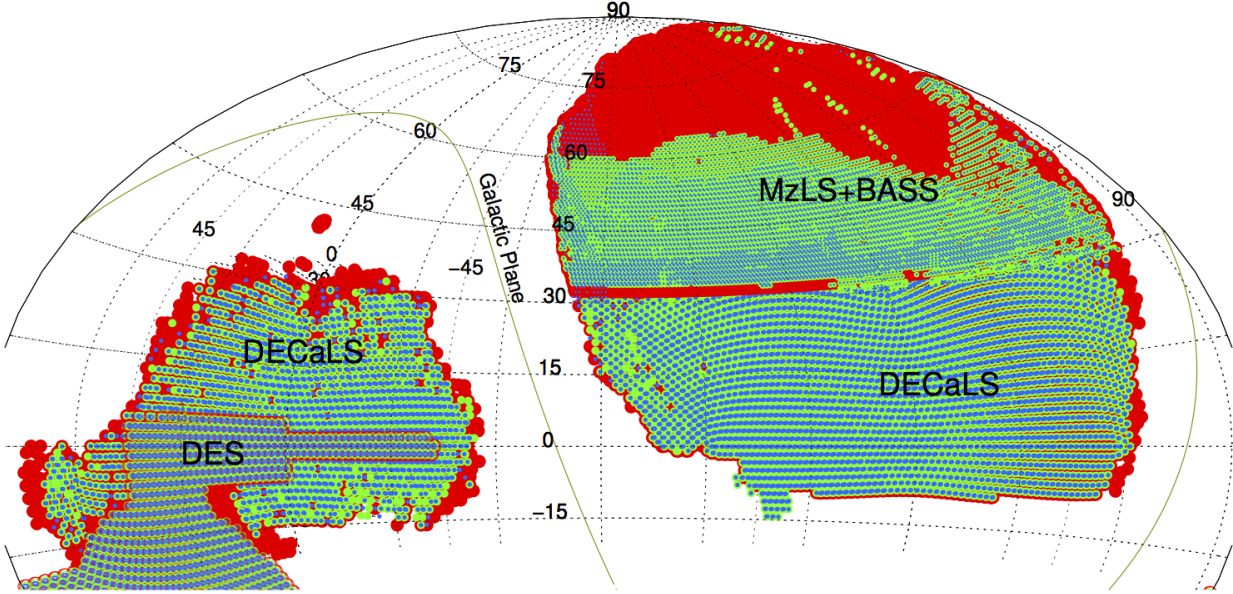


Figure 2. The current imaging coverage (as of April 2018) of the Legacy Surveys. Red, green and blue dots represent regions where there is at least a single z , r or g band observation, respectively. The MzLS z -band survey is now complete; BASS g and r -band observations are expected to be completed in July 2018; and DECaLS is scheduled to complete all grz observations by January 2019. For a more up-to-date status, see <http://legacysurvey.org/status/>.

Consequently, a combination of three telescopes is used to provide the optical imaging for the Legacy Surveys: the Blanco 4-m telescope at Cerro Tololo, the Bok 90-inch and the Mayall 4-m telescope at Kitt Peak (see Table 1). The areas of the Legacy Surveys imaged using each of these telescopes are shown in Figure 1 and the next three subsections discuss these surveys and their current status in more detail. The status of the *WISE* data used in the Legacy Surveys catalogs is presented in § 5.

DESI targeting requires uniformity in the imaging within each sub-footprint, and resorting to multiple platforms poses challenges. In order to minimize non-uniformity and cross-calibration issues, the overall footprint was divided into only three contiguous regions. Two of these three regions are being imaged using the Dark Energy Camera on the Blanco telescope, the instrument and telescope combination delivering the widest field of view (and therefore the fastest survey capability). The other region, which is in the NGC north of $\delta \approx +34^\circ$, is being imaged from Kitt Peak using the 90Prime Camera on the Bok telescope for the g and r bands, and the Mosaic3 camera on the Mayall telescope for the z band observations. The sub-footprints of these individual surveys overlap in the NGC (in an area of $\approx 300 \text{ deg}^2$) in the declination range $+32^\circ < \delta < +34^\circ$, so that the color transformations between the different camera+telescope combinations can be calibrated to high precision and accuracy. An additional $\approx 100 \text{ deg}^2$ in SDSS Stripe 82 is also being imaged by all three surveys to aid the cross-calibration (see Table 2).

A fill factor of unity is not required for the DESI Key Project. As long as the detailed sky mask is well-characterized, the clustering analyses can make use of that mask with information loss proportional to this fractional loss of area. The DESI requirements are that the coverage to full depth in all three optical bands should exceed 90% of the footprint, and that 95% (98%) must be

within 0.3 (0.6) magnitudes of full-depth. The observing nights allocated to each survey are shown in Table 3.

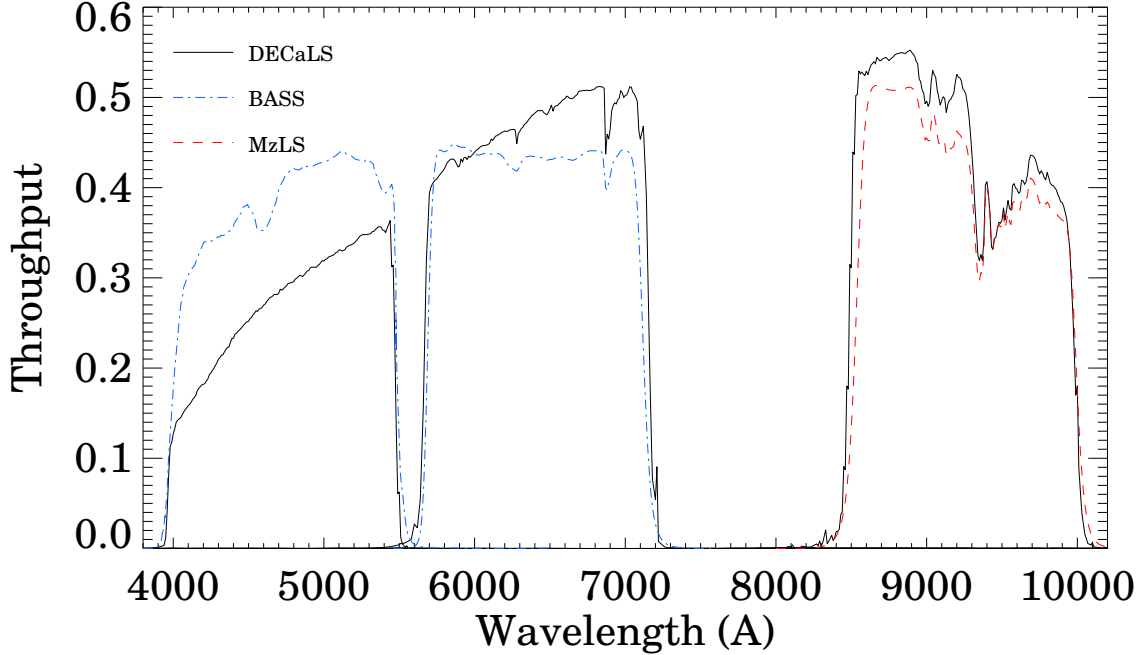


Figure 3. The filter band-passes used for the Legacy Surveys. The DECaLS, BASS and MzLS effective filter throughputs for the entire system are shown as solid (black), dashed (blue) and dot-dashed (red) curves, respectively. These include the transmission of the atmosphere (at a median airmass of 1.1 for BASS and MzLS and of 1.4 for DECaLS), the reflectivity and obscuration of the primary mirror, the corrector transmission, and the quantum efficiency of the CCDs.

Table 1. Telescopes used for the Legacy Surveys

Survey	Telescope/ Instrument	Bands	Area deg ²	Location
DECaLS	Blanco/DECam	g,r,z	9,000	NGC(Dec $\leq +32$ deg)+SGC
BASS	Bok/90Prime	g,r	5,000	NGC (Dec $\geq +32$ deg)
MzLS	Mayall/Mosaic3	z	5,000	NGC (Dec $\geq +32$ deg)
<i>WISE</i> & <i>NEOWISE</i>	<i>WISE</i> W1,W2	3.4,4.6 μm	all-sky	all-sky
<i>WISE</i>	<i>WISE</i> W3,W4	12,22 μm	all-sky	all-sky

4.1. DECaLS: The Dark Energy Camera Legacy Survey

The Dark Energy Camera (DECam; Flaugher et al. 2015) at the 4-m Blanco telescope at the Cerro Tololo Inter-American Observatory is the most efficient imager for wide-field surveys currently

Table 2. Regions where Surveys Overlap

Name	RA	DEC	Area deg ²
D33	100 to 280 to	+32.5 to +34.5	300
S82a	36 to 42	−1.3 to +1.3	13
S82b	350 to 10	−1.3 to +1.3	46
S82c	317 to 330	−1.3 to +1.3	30
COSMOS	330 to 336	−1.3 to +1.3	10

Table 3. Observing Schedule

Survey	Telescope/Instrument	Nights	Start	Finish	Bands
DECaLS	Blanco/DECam	145	2014 Aug	2019 Jan	g, r, z
BASS	Bok/90prime	250	2015 Jan	2019 Jan	g, r
MzLS	Mayall/Mosaic3	383	2016 Feb	2018 Feb	z

Table 4. Depths and Delivered Image Quality

Survey Name	Single-Frame Depths ¹						DIQ		
	PSF Depth ²			Galaxy Depth ³			(")		
	g	r	z	g	r	z	g	r	z
DECaLS ⁴	23.95	23.54	22.50	23.72	23.27	22.22	1.32	1.24	1.14
BASS ⁵	23.65	23.08		23.48	22.87		1.85	1.63	
MzLS ⁶			22.60			22.29			1.16

¹ In AB mag.² Median 5σ detection limit for a point source in individual images.³ Median 5σ detection limit for the fiducial DESI target (galaxy with an exponential disk profile with $r_{\text{half}} = 0.45''$).⁴ From Data Release 5.⁵ From Data Release 6.⁶ Based on all data obtained for the survey.

available. DECam has 62³ 2048x4096 pixel format 250 μ m-thick LBNL CCDs arranged in a roughly hexagonal ≈ 3.2 deg² field of view. The pixel scale is ≈ 0.262 arcsec/pix. In addition to the wide field of view, DECam provides high sensitivity across a broad wavelength range (~ 400 – 1000 nm) and low operational overheads. We are therefore conducting the bulk of the imaging for the Legacy Surveys with DECam. DECam is already being used by the Dark Energy Survey (DES; The Dark Energy Survey Collaboration 2005) to cover ≈ 5000 deg² in the SGC, ≈ 1130 deg² of which lie within the DESI footprint. The Dark Energy Camera Legacy Survey (DECaLS) is targeting the remaining ≈ 9350 deg² (≈ 3580 deg² in the SGC and ≈ 5770 deg² in the NGC). DECaLS was the first of the three

³ One CCD died before the survey, one is only partially usable, and one was inoperative for part of the survey.

Legacy Surveys to begin observations (in August, 2014) and therefore defined the *grz* bandpasses and strategy for the other two surveys described in this section.

For the DECaLS observations we adopt a tiling pattern (from Hardin, Sloane and Smith⁴) which can cover the entire sky with 15,872 tiles and which results in an effective area per tile of 2.60 deg². In order to fill gaps between the CCDs and achieve the required depth across the maximum area, we have chosen three similar, but offset, tiling patterns (labeled Pass 1, Pass 2 and Pass 3). Pass 2 is offset by $(\Delta\alpha, \Delta\delta) = (0.2917^\circ, 0.0833^\circ)$ deg relative to Pass 1; Pass 3 is offset by $(0.5861^\circ, 0.1333^\circ)$. When the survey is complete, approximately 99.97%, 98.00%, 74.33% and 23.8% of the survey will have, respectively, at least 1, 2, 3 and 4 exposure coverage.

DECam can reach the required depths for the fiducial DESI target (see § A) in total exposure times of 166, 134 and 200 sec in *g*, *r*, *z* in median conditions. Accounting for weather loss, DECam is capable of imaging 9000 deg² of the footprint of the Legacy Surveys to this depth in 157 scheduled nights. Observations in the *g* and *r*-band filters are only obtained during dark periods when the moon is below the horizon; *z*-band observations are obtained when the moon is in the sky and during the morning and evening twilight. The DECam observations are conducted using a dynamic observing mode, where the exposure times of an image are scaled to ensure uniform depth to the extent possible (see § 6.2 for details).

“The DECam Legacy Survey of the SDSS Equatorial Sky” (NOAO Proposal ID # 2014B-0404; PI: D. Schlegel and A. Dey), was initially proposed as a public survey beginning in semester 2014A as part of the NOAO Large Surveys programs. This project was initially allocated 64 nights and was aimed at imaging the existing SDSS footprint at $\delta \leq +32^\circ$. The imaging program has been supplemented to a total of 157 scheduled nights (first by NOAO Proposal ID # 2016A-0190, and later using a Director’s allocation) to enlarge the footprint to the full DESI equatorial footprint (i.e., the full region labeled DECaLS in Figure 1). The goal is to complete this survey in the second half of 2018.

The Legacy Surveys program also makes use of other DECam *grz* data within the DESI footprint, as those data become public. The most significant of these other data sets is from the Dark Energy Survey, which includes a 1,130 deg² contiguous area in the SGC footprint of the Legacy Surveys. DECaLS is therefore *not* re-observing that area, and is instead making use of the DES raw data as they become public. Data from the early DECam science verification period has a number of problematic features, and are not currently included in the reductions or data releases from the Legacy Surveys.

4.2. BASS: The Beijing-Arizona Sky Survey

The Beijing-Arizona Sky Survey (BASS; Zou et al. 2017a) is imaging the $\text{DEC} \geq +32^\circ$ region of the DESI North Galactic Cap footprint ($\approx 5,100$ deg²) in the *g* and *r* optical bands. BASS uses the 90Prime camera (Williams et al. 2004) at the prime focus of the Bok 2.3-m telescope. The Bok Telescope, owned and operated by the University of Arizona, is located on Kitt Peak, adjacent to the Mayall Telescope. The 90Prime instrument is a prime focus 8k×8k CCD imager, with four University of Arizona ITL 4k×4k CCDs that have been thinned and UV optimized with peak QE of 95% at 4000 Å (see Williams et al. 2004, for details). These CCDs were installed in 2009 and have been operating routinely since then. 90Prime delivers a 1.12° field of view, with 0.45'' pixels,

⁴ <http://neilsloane.com/icosahedral.codes/>

and 94% filling factor. The median FWHM of the delivered image quality at the telescope is $1.64''$ and $1.86''$ in the g - and r -bands, respectively. The throughput and performance in these bands were demonstrated with data in September, 2013.

BASS tiles the sky in three passes, similar to the DECaLS survey strategy. At least one of these passes is observed in photometric conditions (Pass 1) and seeing conditions better than $1.7''$. Observations in g -band are restricted to dark time, when the moon is below the horizon. The typical individual exposure times are 100 sec per band, with the requirement that 3 passes are needed to reach depth. As in the case of DECaLS, the exposure times are varied depending on the conditions, but limited between 50 sec and 250 sec. We refer the reader to (Zou et al. 2017a) for further details.

BASS was awarded 56/100/100/90 nights in the 2015A/2016A/2017A/2018A semesters (PIs: Zhou Xu and Xiaohui Fan) to target 5500 deg^2 in the NGC and $\approx 100 \text{ deg}^2$ in the SGC.⁵ These areas include $\approx 400 \text{ deg}^2$ of overlap with regions covered by other components of the Legacy Surveys (Table 2) in order to cross-calibrate photometry. Prior to the start of BASS it was determined that the existing Bok g -band filter was well-matched to the DECam g -band filter but the existing Bok r -band filter had a significantly different bandpass. A new r -band filter was therefore acquired from Asahi in April 2015, and was used for subsequent BASS observations.

The BASS survey began observations in Spring 2015. A number of instrument control software updates, new flexure maps, and new observing tools were implemented that greatly improved the pointing accuracy, focusing of the telescope, and observing efficiency. A total of 15% of the g -band and 2% of the r -band tiles were observed in Spring 2015. It was discovered that those data suffered from defective electronics in the read-out system that introduced analog-to-digital conversion errors, gain variations and non-linearities. The 90Prime CCD controller electronics were replaced in September 2015 followed by a recommissioning of the system in Fall 2015.

BASS completed 40% of its expected coverage in 100 scheduled nights in the 2016A semester (January–July). BASS is expected to complete observations by January 2019. As of April 2018, the BASS project has undergone two data releases that are detailed in Zou et al. (2017b,c).

4.3. *MzLS: The Mayall z-band Legacy Survey*

The Mayall z -band Legacy Survey (MzLS) has imaged the $\delta \geq +32^\circ$ region of the NGC footprint of the Legacy Surveys. These z -band observations complemented the BASS g and r band observations in the same $\approx 5,100 \text{ deg}^2$ sub-region of the Legacy Surveys. The delivered image quality at the Mayall telescope is significantly better than that at the Bok telescope (median of $\approx 1.1''$ vs $\approx 1.7''$) and hence the MzLS data are critical to deblending images and to deriving morphologies and source models for the photometric catalogs.

MzLS used the Mosaic3 camera at the prime focus of the 4-meter Mayall telescope at Kitt Peak National Observatory. In 2015, prior to the commencement of MzLS, the Mayall 4-m telescope's prime focus imaging system underwent a major upgrade aimed at improving its z -band efficiency. Details of the Mosaic3 camera upgrade are presented in Dey et al. (2016); here, we briefly describe the main modifications to the system.

The Mosaic-3 camera is a new version of the prime focus imaging system at the Mayall 4-m telescope. The previous version, known as Mosaic-1.1, was a blue-sensitive camera equipped with eight thinned $2048 \times 4096 \text{ } 15\mu\text{m}$ pixel format e2v CCDs. The camera had a twin, Mosaic-2, at the Blanco telescope

⁵ see <http://batc.bao.ac.cn/BASS>

at CTIO, which was decommissioned and replaced with the Dark Energy Camera. The Mosaic-3 upgrade repurposes the dewar from the CTIO Mosaic-2 camera, while retaining the rest of the Mosaic-1.1 mechanical system and guider. Yale University designed and built a new cold plate for the dewar, which was populated with four ($500\mu\text{m}$ -thick) fully-depleted LBNL 4096×4096 $15\mu\text{m}$ pixel CCDs. The new readout system consists of four prototype DESI controllers, one for each CCD, that are synchronized to a single clock in order to simultaneously read the four quadrants of each device. The dewar was delivered to NOAO in September 2015 where it was integrated with the Mosaic-1.1 mechanical enclosure, shutter, filter wheel and acquisition and guider system. NOAO also purchased a new z -band filter, matched to the DECam filter bandpass, in order to minimize any differences between the DECam and Mosaic3 z surveys. In addition, the KPNO 4-m telescope control system and the imaging camera software were upgraded for improved operational efficiency (Abareshi et al. 2016; Dey et al. 2016). Mosaic3 saw first light in October 2015 and underwent further on-sky commissioning runs in November and December 2015. The z -band efficiency is measured to be 60% better than that of its predecessor, the Mosaic-1.1 camera.

The MzLS survey uses a 3-pass strategy, similar to DECaLS, and tiles the sky with $\approx 122,765$ tiles per pass. Pass 1 is observed only in photometric conditions and seeing conditions better than 1.3 arcsec. For 1.3 arcsec seeing and a sky brightness of 18.2 AB mag/arcsec², the total time required is 200 sec (≈ 67 sec per exposure) in z . As in the case of DECaLS, we limited the exposure times for individual exposures to be in the range $80 \leq t_{\text{exp}} \leq 250$ sec. Observations were made during all lunar phases, although during bright time we limited our observations to regions of the footprint lying >40 – 50 deg away from the Moon.

MzLS began official survey operations on February 2, 2016, and ended on February 12, 2018. During this period, MzLS used a total of 382.7 nights, 276.8 of which were clear enough to allow observations. During the second semester of observing (2017A), MzLS progress slowed because of poor weather and instrumental and operational problems.

The Mosaic3 camera was decommissioned and the Mayall telescope shut down on February 12, 2018 to prepare for the installation of the DESI instrument.

5. WISE DATA

The Legacy Surveys source catalogs include mid-infrared photometry from the *Wide-field Infrared Survey Explorer* (*WISE*) satellite for all optically detected sources. Mid-infrared imaging is critical to the DESI targeting algorithms for luminous red galaxies (LRGs) and quasars (QSOs). During its primary 7-month mission from 2010 January through 2010 August, *WISE* conducted an all-sky survey in four bands centered at 3.4, 4.6, 12 and $22\mu\text{m}$ (known as W1, W2, W3 and W4; Wright et al. 2010; Cutri et al. 2012). Following its primary 4-band mission, *WISE* continued survey operations in the three bluest bands for 2 months, then the two bluest bands for an additional 4 months, resulting in a combined 13-month mission that completed in 2011 February. Through a mission extension referred to as *NEOWISE-Reactivation* (*NEOWISE-R*; Mainzer et al. 2014), NASA reactivated the satellite and resumed 2-band survey observations on 2013 December 13. *NEOWISE-R* observations remain ongoing. The first, second and third annual *NEOWISE-R* data releases, which each consist of single-exposure (Level 1b) images and source extractions, occurred on 2015 March 25, 2016 March 23 and 2017 June 1.

DESI target selection utilizes the two shortest-wavelength bands at $3.4\mu\text{m}$ (W1) and $4.6\mu\text{m}$ (W2). Photometry in these bands is measured using *The Tractor* algorithm (see Section 8), adopting source

centroid and morphology parameters from the optical imaging, which has much better angular resolution than *WISE*. *The Tractor* measurements are based on custom stacks of *WISE/NEOWISE* exposures which are optimized for forced photometry and therefore preserve the native *WISE* resolution. These stacks are referred to as unWISE coadds (Lang 2014). DR1 made use of the Lang (2014) unWISE coadds based on the initial 13-month *WISE* data set, reaching 5σ limiting magnitudes of 20.0 and 19.3 AB mag in W1 and W2. DR2 and DR3 made use of approximately twice as much W1/W2 data by incorporating photometry measurements from stacks of *WISE* and the first year of *NEOWISE-R* exposures (Meisner et al. 2017b). DR4 and DR5 photometered image stacks that folded in the second year of *NEOWISE-R* imaging (Meisner et al. 2017a), resulting in depth enhancements of 0.56 (0.46) magnitudes relative to DR1 in W1 (W2). DR6 incorporates all publicly available *WISE* and *NEOWISE-R* imaging, including that from the third-year *NEOWISE-R* release (Meisner et al. 2018). The final catalogs from the Legacy Surveys will push even deeper at 3–5 μm by leveraging the full *WISE* and *NEOWISE-R* data sets.

In addition to the mid-infrared photometry measured from the “full-depth” W1/W2 unWISE stacks (which are required for DESI targeting), the Legacy Surveys DR3–DR6 also include W1/W2 forced photometry light curves corresponding to all optically detected sources. These light curves are measured from time-resolved unWISE coadds similar to those described in Meisner et al. (2017c). Such light curves provide variability information on all optically-detected sources, which can be used, among other things, for the DESI quasar selection, although this possibility has not yet been tested in detail. The Legacy Surveys DR3 (DR4–DR6) W1/W2 light curves typically have 4–5 (6–7) coadded epochs per band.

6. OBSERVATIONS

In this section, we briefly describe the observing strategy employed by the Legacy Surveys. For a more detailed description of the implementation and algorithms, we refer the reader to Burleigh et al. (2018).

6.1. Survey Strategy

As described in §4, all three surveys (DECaLS, BASS and MzLS) use a 3-pass strategy to tile the sky. This strategy is designed to account for the gaps between CCDs in the cameras, ensure that the surveys reach the required depth, remove particle events and other systematics, and ensure photometric and image quality uniformity across the entire survey. In order to calibrate the entire survey photometrically, we place requirements on the minimum observing conditions needed for each pass. Pass 1 tiles are only observed when the conditions are photometric (defined as the transparency being better than 90% and the sky being clear) and when the seeing is better than a specified limit (1.3'' for DECaLS and MzLS; 1.7'' for BASS). If only one of these conditions is met (i.e., seeing < 1.3''/1.7'' or photometric), then we observe pass 2; if both are not met, we observe pass 3. The successful implementation of this strategy guarantees that we have at least one photometric and good-seeing image at every sky position, which can be used to calibrate the photometry across the entire survey footprint.

The determination of whether the conditions are photometric and the seeing measurements are made “on-the-fly” at the telescope, using a combination of the on-site telemetry, the observer’s periodic visual inspection of the sky, and quick analyses of every frame. At the Blanco telescope, the observers determine which pass to observe using the output of the Radiometric All-Sky Infrared

Camera (RASICAM; Reil et al. 2014), the CTIO All-Sky Camera⁶, the output of the DECam “ken-tools” (created by S. Kent) and our own custom software. Our software identifies stars, matches to the PS1 Data Release 1 (DR1) catalog, and measures the seeing, transparency, sky brightness and positional offset of the telescope from the desired pointing center. At the Mayall and Bok telescopes, the observers determine which pass to observe using the KPNO All-Sky Camera, weather satellite maps, and our own custom software⁷.

6.2. *Dynamic Observing*

In order to optimize the observing efficiency and create as uniform a survey as possible, we have implemented an observing mode which adjusts the exposure time dynamically. The observing strategy is described in detail in Burleigh et al. (2018), but here we provide a brief overview.

The desired target depth of each exposure is defined as that for which the fiducial DESI target galaxy (see § A) is detected with a signal-to-noise ratio of at least $5/\sqrt{2}$ (i.e., that the survey reaches the requisite depth with two passes). To ensure that each image of the sky reaches the desired depth, we implement the following procedure. We plan image exposure times based on knowledge of the target field’s interstellar dust reddening, its position on the sky at the likely time of observation (which determines the likely atmospheric extinction, sky brightness, and modulates the seeing), and estimates of the observing conditions. As soon as an image is taken and written to disk, a sample CCD (or single amplifier of a CCD) is analyzed: sources are detected and their positions are cross-matched with a stellar catalog derived from the PS1 survey. This analysis produces estimates of the seeing, transparency (estimated by comparing the measured zeropoint with the fiducial photometric zero point of an observation through clear skies), the telescope pointing error, the sky brightness and the resulting depth reached for the canonical DESI galaxy target. These measurements allow us to update the exposure time of subsequent observations to ensure that we reach the required depth. Exposure times are not allowed to fall below a minimum value in order to limit the overhead⁸. Additionally, exposure times are limited to a maximum value defined by the minimum of t_{sky} and t_{max} , where t_{sky} is the exposure time at which the sky counts = 20,000 adu, and t_{max} is a fixed maximum exposure time (e.g., t_{max} is [200,175,250] sec for DECam [g,r,z] observations, respectively).

In practice, it takes a minimum lag of two exposures to update the queue with an observation that has a modified exposure time. At the Blanco, this lag was driven by the need to keep at least two exposures in the active queue to avoid stopping the queue inadvertently, and at the Mayall the transfer of images and the subsequent analyses resulted in this lag. Even with the current implementation, the result is a relatively uniform survey product (see Burleigh et al. 2018, for details about the algorithms used and the implementation).

7. DATA REDUCTION AND CALIBRATIONS

All data from the Legacy Surveys are first processed at NOAO/Tucson through the NOAO Community Pipelines (“CPs”). Each instrument and telescope combination has its own CP that takes raw data as an input and provides detrended and calibrated data products. The NOAO Pipeline Scientist and architect is co-author F. Valdes, who is responsible for the development and continued operation of the CPs. The CPs include algorithms and code (from a variety of sources) which are

⁶ <http://www.ctio.noao.edu/noao/content/tasca-latest-image>

⁷ <https://github.com/legacysurvey/obsbot>.

⁸ For example, for DECam, these were initially defined as 50, 50, and 100 sec for g,r,z respectively; after 2016-07-20, the minimum exposure time in g was increased to 70 sec.

modified and packaged for the needs of the NOAO environment and characteristics of the different instruments. A common feature of all the CPs is the orchestration framework (The NOAO High Performance Pipeline System: Scott et al. (2007)) that allows parallelized processing across the NOAO computing resources to handle the large volumes of data produced by NOAO observing programs.

The CPs provide instrumentally calibrated data products for observers, programs, and archival researchers. Instrumental calibrations include: typical CCD corrections (e.g., bias subtraction and flat fielding); astrometric calibration (e.g., mapping the distortions and providing a world coordinate system, or WCS); photometric characterization (e.g., magnitude zero point calibration); and artifact identification, masking and/or removal (e.g., removal of cross-talk and pupil ghosts, and identification and masking of cosmic rays). Data products delivered to the NOAO Science Archive include flux calibrated images (i.e., individual images with and without distortion corrections applied, and image stacks), bad data masks, and weight maps.

The three cameras used by the Legacy Surveys (i.e., DECam, Mosaic3, and 90Prime) each have their own CP. The basic steps of each CP are summarized in Table 5. Detailed technical descriptions of each CP are in preparation⁹ (Valdes et al. 2014, describes an early version of DECam CP). Some calibrations are not perfect, with the detection and masking of artifacts being only partially effective and background pattern subtraction around very large and bright sources being prime examples. In particular, the CP can result in unmasked spurious sources in the final catalogs. First, the thick, deep depletion LBNL CCDs employed in the DECam and Mosaic3 cameras are excellent detectors of particle events (see Groom 2004, for a more detailed discussion), a fraction of which are inadequately masked by the current CP. Second, asteroids and other moving targets are not flagged by the CP and will appear as detected sources in the final catalogs.

The CP-calibrated individual images, bad pixel masks and weight maps are transferred to the National Energy Research Scientific Computing Center (NERSC), where post-processing is done in order to improve the astrometric and photometric calibrations and create the source catalogs. Similarly, the *WISE* satellite data are transferred to NERSC as they become public, and new coadded stacks are constructed on an approximately yearly basis.

7.1. Astrometric Calibration

The NOAO CP reductions of all Legacy Survey imaging data derive a world coordinate system (WCS), a function mapping pixel coordinates to celestial coordinates. The function (TPV: tangent plane projection with polynomial distortions¹⁰) is determined for each CCD by least square fitting to the pixel centroids of detected sources with known coordinates in a reference catalog.

The reference coordinates were from the 2MASS catalog (Skrutskie et al. 2006) for DECam data from 2013 and 2014; later DECam data and all Mosaic3 and 90Prime data use the Gaia DR1 catalog (Gaia Collaboration et al. 2016a). Since the calibration procedure ties source positions in each exposure to celestial sources, it effectively includes calibration for the atmospheric distortions (at some mean color) and, in the case of the Bok 90Prime data, correction for distortions resulting from the focusing procedures.

While this procedure corrects the data for global distortions (the TPV solutions are continuous and smooth across an individual CCD), it does not correct for some small-scale effects. For example,

⁹ A draft on-line DECam CP description is https://www.noao.edu/noao/staff/fvaldes/CPDocPrelim/PL201_3.html

¹⁰ <https://fits.gsfc.nasa.gov/registry/tpvwcs/tpv.html>

Table 5. Calibration Steps in the NOAO Community Pipelines

#	Calibration	DECam	BASS	MzLS
1.	Linearity correction	✓		
2.	Cross-talk subtraction	✓	✓	✓
3.	Overscan & bias subtraction	✓	✓	✓
4.	Dome flat fielding	✓	✓	✓
5.	Amplifier gain balancing ¹	✓	✓	✓
6.	Masking of bad pixels ²	✓	✓	✓
7.	Interpolation over bad/saturated pixels ³	✓	✓	✓
8.	Correction of line shifts ⁴		✓	✓
9.	Astrometric calibration ^{5,6}	✓	✓	✓
10.	Removal of sky patterns/gradients	✓	✓	✓
11.	Pupil ghost subtraction	✓	only <i>g</i> -band	✓
12.	Fringe-pattern removal ⁷	only <i>z</i> -band	only <i>r</i> -band	✓
13.	Illumination correction (sky flat)	✓		
14.	Removal of pattern/stripping noise		✓	✓

¹DECam uses starflats and BASS/MzLS uses PS1. For MzLS the gain balancing is a function of the sky level.

²Bad pixels are detector defects, saturated, bleed trails, cosmic rays, and satellite trails.

³Stellar cores are masked but not interpolated.

⁴Some MzLS data suffered from 1/3-pixel shifts and dropped columns and BASS has systematic centroid shift due to CTE.

⁵DECam is referenced to a mixture of 2MASS and Gaia DR1. BASS and MzLS are referenced only to Gaia DR1.

⁶DECam has a fixed distortion map with 2nd order adjustments. BASS and MzLS have full 4th order solutions.

⁷Implemented for DECam only in 2018, and so far only applied to the 2018 observations.

the DECam and Mosaic3 CCDs are known to have very small scale distortions known as “tree rings” (Plazas et al. 2014), and the Mosaic3 CCDs show a residual astrometric pattern from bonding stresses. Differential chromatic refraction is also not accounted for in the astrometric solutions (e.g., see Bernstein et al. 2017, for an excellent discussion of issues affecting the DECam astrometry). These combined effects affect the astrometric accuracy at the level of $\approx 10 - 30$ mas and are currently not corrected in the post-processing catalog generation step.

In addition, the Mosaic3 electronics occasionally read out with a missing starting column. The CP detects and corrects this; however, since the edges are masked anyway this has no effect on the astrometry. Prior to MJD 57674 the readout electronics introduced a one-third pixel shift between amplifiers in the vertical transfer direction (corresponding to the east-west direction on the sky). Since this is a precise, discrete offset the CP corrects this completely with no effect on the astrometry.

90Prime has charge transfer effects that affect centroid measurement and, in particular, introduce systematic opposing shifts between amplifiers in the serial transfer direction. The systematic offset

between the two halves is ≈ 160 mas for CCD-1 and ≈ 70 mas for the other 3 CCDs. These corrections are applied by the CP to each exposure and they substantially reduce, but do not completely remove, this systematic effect.

As noted earlier, the CP data is only the first part of the Legacy Surveys calibrations. Small residual mean offsets per CCD are applied to the CP astrometric zeropoint calibrations using a reference catalog constructed from stars color-selected from the PS1 DR1 catalog (Chambers et al. 2016) with positions from the Gaia DR1 catalog (Gaia Collaboration et al. 2016a). For all releases prior to (and including) DR3 of the Legacy Surveys, astrometric and photometric calibration is based on comparisons to a subset of PS1 catalog sources with magnitudes < 21.5 AB mag and colors $0.4 < (g - i)_{\text{PS1}} < 2.7$ AB mag. Starting with DR4 of the Legacy Surveys, PS1 positions of these sources were replaced with the Gaia DR1 catalog positions; i.e. post-DR3 astrometry is tied to Gaia. The astrometric residuals for bright stars relative to Gaia are shown in Figure 4, 5 and 6. MzLS and DECaLS have rms scatters of ≈ 20 mas, with BASS showing slightly larger residuals. The asymmetries visible in Figures 4 and 6 are due to pixel-level distortions on the deep depletion CCDs used in the Mosaic3 and DECam cameras, and these offsets will be incorporated into *The Tractor* modeling in future data releases.

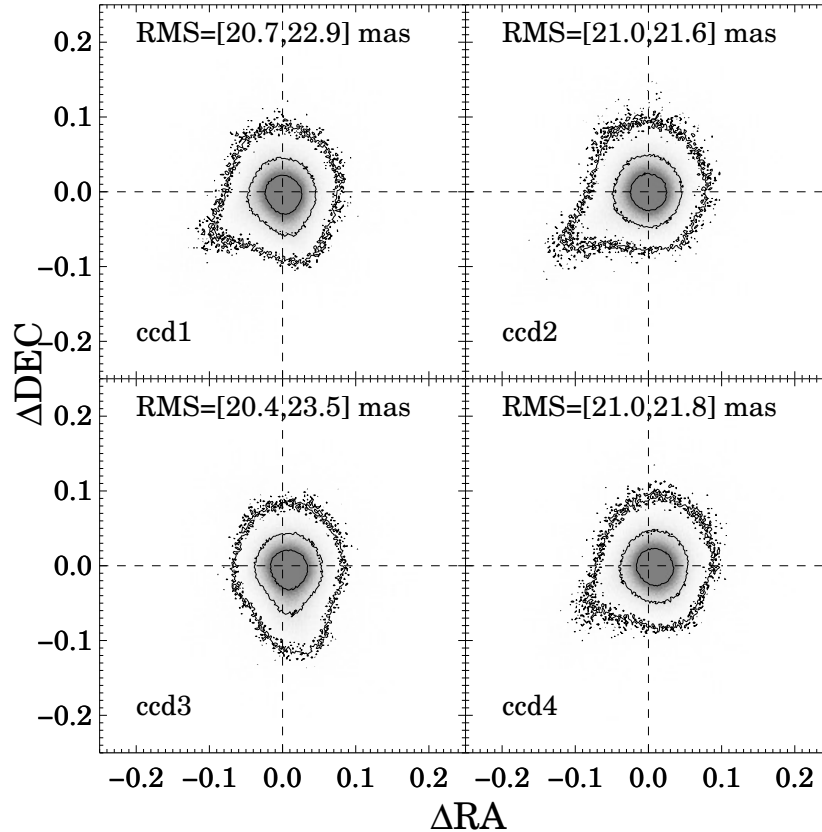


Figure 4. The astrometric precision of the four Mosaic3 CCDs, computed by matching stars detected in the MzLS images with those in Gaia DR1 catalog. In each panel, the greyscales show the distribution of the differences (in units of arcseconds) between the derived positions (using the WCS) of the centroids of bright stars on a Mosaic3 CCD and their positions in the Gaia DR1 catalog.

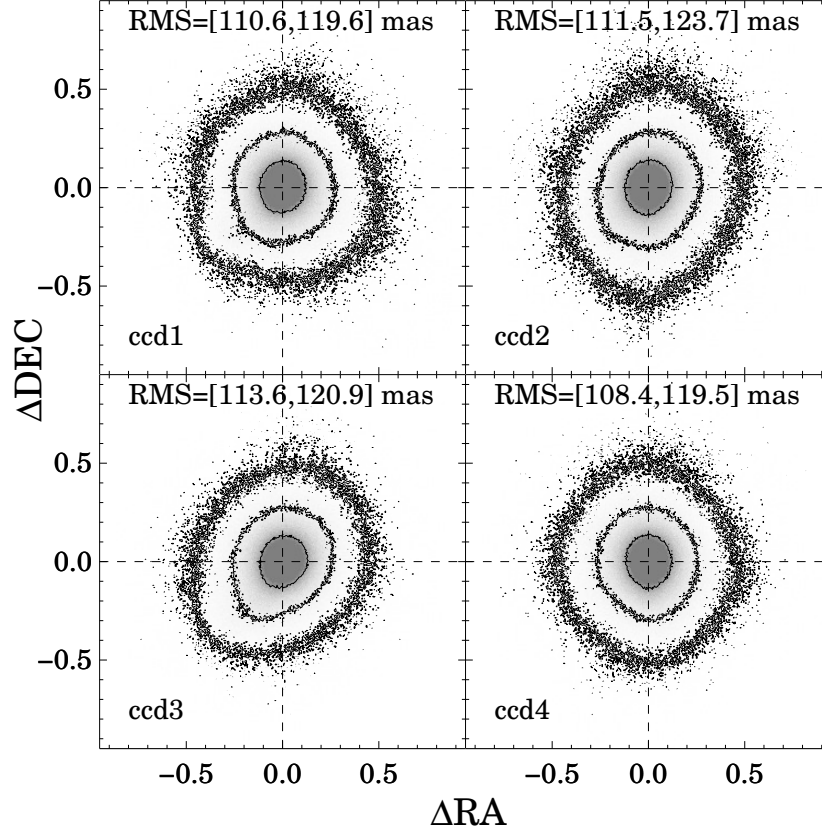


Figure 5. The astrometric precision of the four Bok 90Prime CCDs, computed by comparing the derived positions (using the WCS) of bright stars with their positions in the Gaia catalog.

7.2. Photometric Calibration

The role of the CPs in photometric calibration is to provide a spatially uniform gain upon which later absolute calibrations can focus on the CCDs as a whole. The CPs also provide the data quality masks and weight maps which are used for in the subsequent source detection and photometric calibration steps.

The Legacy Surveys are designed so that each part of the footprint is observed in photometric conditions at least once, and most of the footprint is observed in photometric conditions two or more times. Efforts to observe at the lowest possible airmasses and avoid the Moon drive an observing plan that features a rich set of overlaps between observations on different nights. Comparison of observations of the same stars on different nights and at different airmasses then enables determination of the system throughput and the transparency of the atmosphere for each photometric night of the survey. This procedure is the basis of the photometric calibration of the SDSS (Padmanabhan et al. 2008), as well as subsequent surveys like PS1 (Schlafly et al. 2012) and DES (Burke et al. 2018). Observations on non-photometric nights will be calibrated by matching directly to overlapping observations taken on photometric nights.

The current photometric calibration for the Legacy Surveys (for all data releases through DR6) is, however, tied to the PS1 DR1 photometry through a set of color transformation equations. The

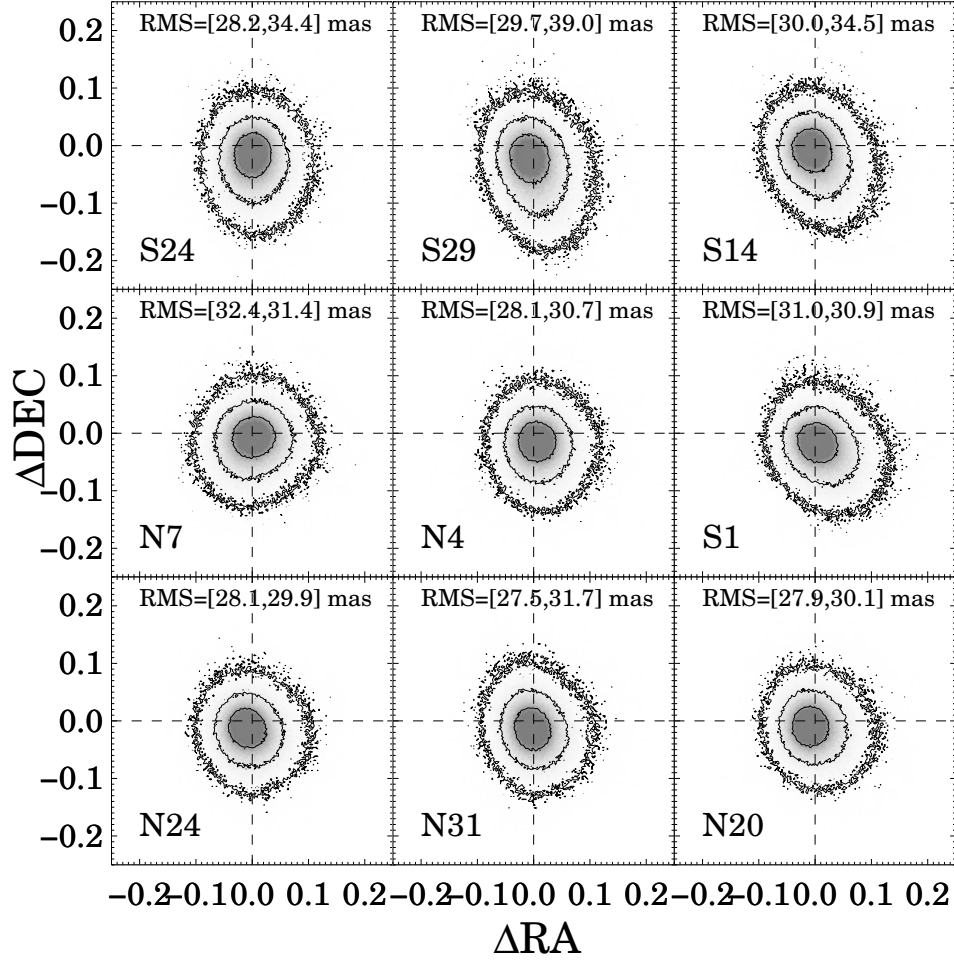


Figure 6. The astrometric precision of the DECaLS CCDs, computed by comparing the derived positions (using the WCS) of bright stars with their positions in the Gaia catalog. The N4 CCD is one of two central CCDs in the DECam mosaic; the other 8 CCDs shown are edge CCDs in the mosaic and represent regions with the largest astrometric and PSF distortions.

magnitudes of PS1 DR1 catalog sources are first converted to the “native” system for each telescope+camera+filter, and the transformations are as follows:

$$g_{\text{DECaLS}} = g_{\text{PS1}} + 0.00062 + 0.03604(g - i)_{\text{PS1}} + 0.01028(g - i)_{\text{PS1}}^2 - 0.00613(g - i)_{\text{PS1}}^3 \quad (1)$$

$$r_{\text{DECaLS}} = r_{\text{PS1}} + 0.00495 - 0.08435(g - i)_{\text{PS1}} + 0.03222(g - i)_{\text{PS1}}^2 - 0.01140(g - i)_{\text{PS1}}^3 \quad (2)$$

$$z_{\text{DECaLS}} = z_{\text{PS1}} + 0.02583 - 0.07690(g - i)_{\text{PS1}} + 0.02824(g - i)_{\text{PS1}}^2 - 0.00898(g - i)_{\text{PS1}}^3 \quad (3)$$

$$g_{\text{BASS}} = g_{\text{PS1}} + 0.00464 + 0.08672(g - i)_{\text{PS1}} - 0.00668(g - i)_{\text{PS1}}^2 - 0.00255(g - i)_{\text{PS1}}^3 \quad (4)$$

$$r_{\text{BASS}} = r_{\text{PS1}} + 0.00110 - 0.06875(g - i)_{\text{PS1}} + 0.02480(g - i)_{\text{PS1}}^2 - 0.00855(g - i)_{\text{PS1}}^3 \quad (5)$$

$$z_{\text{MzLS}} = z_{\text{PS1}} + 0.03664 - 0.11084(g - i)_{\text{PS1}} + 0.04477(g - i)_{\text{PS1}}^2 - 0.01223(g - i)_{\text{PS1}}^3 \quad (6)$$

These calibrations were determined using the CALSPEC database¹¹ (see Bohlin et al. 2017, and references therein). The DECaLS transformations used above are the same as those determined by Schlafly et al. (2018) for the DECaPS Galactic Plane Survey. The BASS and MzLS transformations were determined in a similar manner, using unresolved sources selected from PS1 DR1 with well-measured photometry (i.e., no flags) with colors in the range $0 < (g - i)_{\text{PS1}} < 2.9$. Constant terms in the calibration are intended to place the Legacy Surveys on the AB magnitude system (Oke & Gunn 1983), and were derived from comparison of the empirical transformations with synthetic transformations of calibrated Hubble Space Telescope standard stars, given the system throughputs of the DECam, BASS, and MzLS surveys. (The photometric transformations between the SDSS *grz* magnitudes and the Legacy Surveys’ magnitudes are presented in Appendix B.)

We estimate a zero point for each CCD independently, by (1) detecting sources on the pipeline-reduced data; measuring their instrumental magnitudes; (2) matching to the subset of PS1 DR1 catalog sources selected as calibrators; and then (3) comparing the instrumental magnitudes to the color-transformed PS1 DR1 magnitudes (i.e., as per Equations 1–6). This procedure results in zeropoints for each CCD tied to the global PS1 calibration, but corrected to the “native” photometric frame for each individual survey.

In the future, we will migrate to an internal photometric calibration that will rely solely on data from each of the Legacy Surveys. The large network of repeat observations on different photometric nights enables the construction of a detailed description of the throughput of the various imaging systems used in the Legacy Surveys. We plan to not only measure overall system zeropoints and (grey) atmospheric transparency in each band on each night (cf., Padmanabhan et al. 2008), but also to determine how sensitivity varies within and among the different CCDs of each system as a function of time, (cf. Schlafly et al. 2012, 2018). We can also determine and ameliorate systematic problems with aperture correction. Well-calibrated optical colors are now available from PS1 and Gaia, which will make it straightforward to remove systematic chromatic errors stemming from the different colors of stars and the varying effective throughput of the imaging system in different conditions (Li et al. 2016; Burke et al. 2018). Initial results for DECam suggest that we will be able to obtain < 5 mmag photometric precision for typical stars.

8. INFERENCE MODELING WITH *THE TRACTOR*

Co-author D. Lang has developed *The Tractor*¹² as a forward-modeling approach to perform source extraction on pixel-level data. This algorithm is a statistically rigorous approach to fitting the differing PSF and pixel sampling of the different imaging data that comprise the Legacy Surveys. This is particularly important, given that the optical data have a typical PSF of ≈ 1 arcsec and the *WISE* PSF FWHM is ≈ 6 arcsec in W1–W3 and ≈ 12 arcsec in W4.

The Tractor takes as input the individual images from multiple exposures in multiple bands, with different seeing in each. For each astronomical source, a source model is fit simultaneously to the pixel-level data of all images containing the source. For the Legacy Surveys, we have created the *legacypipe* pipeline software¹³, wrapping *The Tractor*, as follows. We construct initial image stacks using weighted sums of the optical (i.e., *grz*) images. Each individual image is first convolved with its PSF model and we then create image stacks for each individual band. We also construct two

¹¹ Specifically, the November 2017 version of the release. See <http://www.stsci.edu/hst/observatory/crds/calspec.html> for details.

¹² Publicly available at <https://github.com/dstndstn/tractor>

¹³ Publicly available at <https://github.com/legacysurvey/legacypipe>

different image stack combinations using all three bands to optimize for two generic types of spectral energy distributions (SED): (1) a “flat” SED (i.e., zero AB mag color); and (2) a “red” SED (i.e., with colors $g-r = 1$ mag and $r-z = 1$ mag). Next, we detect sources on the individual-band image stacks and the two grz image stacks using a simple thresholding algorithm, selecting sources above 6σ . This process identifies almost all sources in the images to faint magnitudes.

We then model each source using a small set of parametric light profiles: a delta function (for point sources); a deVaucouleurs $r^{-1/4}$ law; an exponential disk; or a “composite” deVaucouleurs plus exponential. The best fit model is determined by convolving each model with the specific PSF for each individual exposure, fitting to each image, and minimizing the residuals for all images. The PSF for each optical image is constructed using PSFEx (Bertin 2011). We make the assumption that the model is the same across all the bands. Thus, if a source is determined to be a point source, it is modeled as a point source in every band and every exposure and its catalog photometry is based on this model. Alternatively, if the source is spatially extended, then the same light profile (an exponential disk, de Vaucouleurs, or combination) is consistently fit to all images in order to determine the best-fit source shape parameters and photometry¹⁴.

The Tractor model fits are determined using only the optical grz data. The mid-infrared photometry for each optically-detected source is then determined by forcing the location and shape of the model, convolving with the *WISE* PSF and fitting to the *WISE* stacked image. This “forced photometry” approach allows us to deblend any confused *WISE* sources by using the higher-spatial-resolution optical data, but also limits the Legacy Surveys catalogs to only contain *WISE* photometry for sources that are detected at optical wavelengths. The procedure described produces object fluxes and colors that are consistently measured across the three Legacy Surveys.

Figure 7 shows examples of how *The Tractor* is being applied to the Legacy Surveys. The footprint of the Legacy Surveys is divided into “bricks” of size $0.25^\circ \times 0.25^\circ$, and a model of the sky within each brick is computed using all CCDs that contribute data within that brick. The three sets of vertical panels show: the grz image data for a brick; the rendered *The Tractor* model; and the residual image (i.e., data – model). While most of the faint sources are well fit by the parametric models we used for DR5 and DR6 of the Legacy Surveys, more significant residuals are seen associated with very extended galaxies and the halos of bright, saturated stars.

The Tractor and our source detection algorithms do result in the catalog containing a small fraction of spurious sources. These are primarily due to inadequately masked particle events or satellite trails, single-exposure detections of transient sources (primarily asteroids), and sources identified in the extended scattered light halos or diffraction spikes associated with bright stars, or in the diffuse emission associated with large galaxies. In addition, spatially large, extended sources with complex morphologies (e.g., large galaxies) and crowded fields (e.g., globular clusters and open star clusters) are poorly modeled by *The Tractor*. Finally, a small number of sources are missed by *The Tractor* catalog; these are primarily very low surface brightness diffuse sources or sources lying close to a (typically brighter) star or galaxy.

The “forced photometry” approach we use to measure the mid-infrared photometry from the *WISE* images allows us to detect fainter sources than a traditional approach while preserving the photometric reliability. For bright objects that were cleanly detected by *WISE* alone (and recorded in

¹⁴ Further details regarding the catalog construction and source parameter extraction can be found at the Legacy Surveys’ website describing the latest data release.

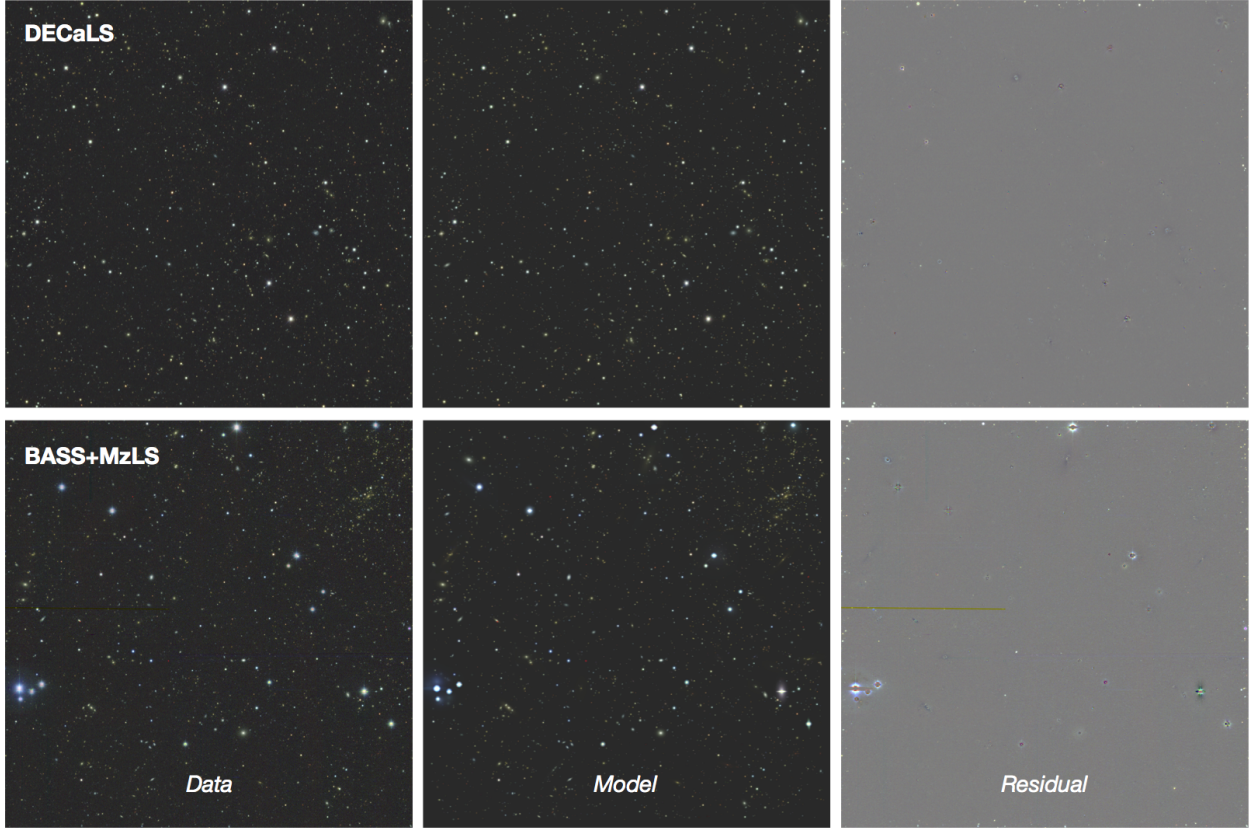


Figure 7. Example “bricks” covering $0.25 \times 0.25 \text{ deg}^2$ from the DECaLS survey (top row; brick 2212p085) and the MzLS and BASS surveys (bottom row; brick 1689p532). From left to right, the panels show the actual *grz* imaging data, the rendered model based on *The Tractor* catalog of the region, and the residual map. *The Tractor* catalog represents an inference-based model of the sky that best fits the observed data.

the AllWISE catalog), the pixel-level measurements are consistent with catalog-level measurements (see Figure 8, left panel). However, we are also able to measure the fluxes of significantly fainter objects, as well as study collections of objects that are blended in the *WISE* images but that are resolved in the optical images. The increased level of source counts in the force-photometered data observed at bright *WISE* magnitudes (i.e., $W1 \lesssim 16 \text{ mag}$) in the right panel of figure 8 is due to sources detected in the vicinity of bright stars or galaxies; $\approx 50\%$ of these sources are real objects, and the remaining are spurious detections due to the halos or diffraction spikes around bright stars or the poorly-modeled extended light of galaxies. All are located near other brighter targets, which is why they are compromised. We are currently working on improving the models for future data releases. Figure 9 compares a traditional optical-infrared color-color diagram, based on matching sources between catalogs at different wavelengths, to the photometry derived from our *WISE* forced photometry, which requires no such matching. This demonstrates how *The Tractor* greatly increases the access to mid-infrared photometry for targets fainter than the AllWISE catalog detection limits, albeit with increased scatter.

The Tractor should improve target selection for all DESI target classes by allowing information from low signal-to-noise ratio measurements to be utilized. *The Tractor* is particularly important for

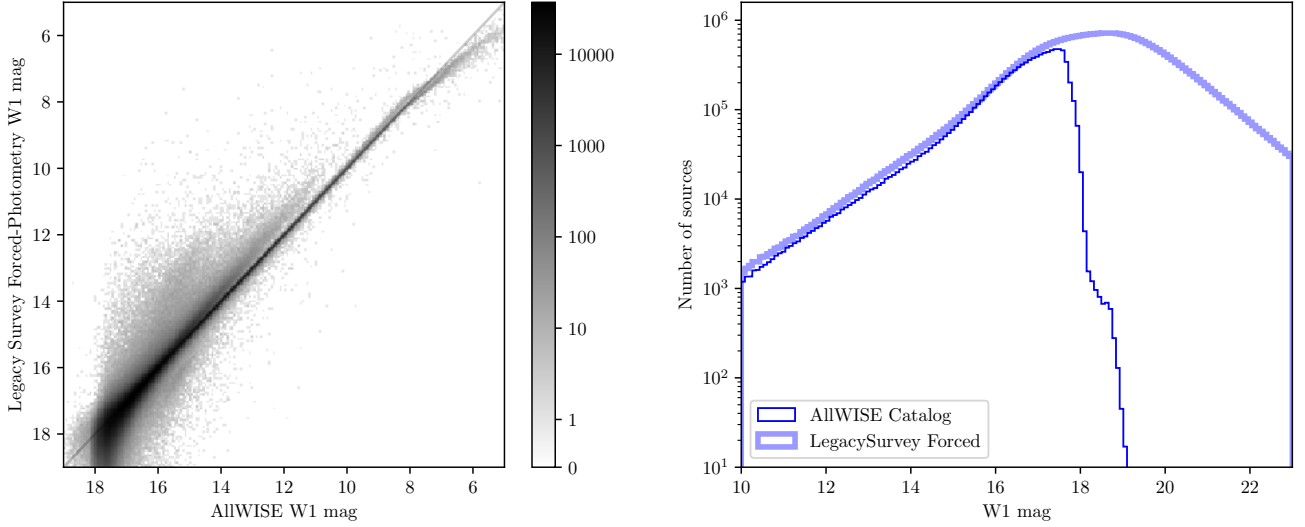


Figure 8. Forced photometry with *The Tractor* code, using information from Legacy Surveys detections and light profiles, allows us to measure the mid-infrared flux from objects in the *WISE* images to below the *WISE* detection limit. *Left panel:* A comparison of the *W1* photometric measurements in the Legacy Surveys’ catalog (derived using *The Tractor*) with those in the ALLWISE catalog; the greyscale shows the relative density of points. The photometry agrees well for mid-infrared bright objects that are detected in the AllWISE catalog. The widening locus below $W1 \sim 14$ is due to *The Tractor* photometry treating larger objects as truly extended, in contrast to the point-source-only assumptions in the public AllWISE catalog. *Right panel:* The number counts in the Legacy Surveys’ catalog compared with those from AllWISE, demonstrating the increased depth made possible from using *The Tractor*. By using optical imaging from Legacy Surveys to detect objects, photometry is measured for objects that are well below the detection limit of the AllWISE catalog.

targeting QSOs. Up to 15% of QSO spectra exhibit broad absorption lines that potentially reduce the measured flux in broad-band imaging. In addition, high-redshift QSOs at $z \geq 5.0$ (≥ 6.9) will drop out of the *g*-band (*g*- and *r*-bands) completely (e.g., see Bañados et al. 2018). Finally, the 5σ optical limit at the extremes of DESI targeting corresponds to a $< 5\sigma$ limit in *WISE* for QSOs. *The Tractor* successfully differentiates between the QSOs that are detected in *WISE*, and the QSOs that in general are not detected, whereas traditional “catalog-matching” approaches would not be successful.

The SDSS-IV/eBOSS (Dawson et al. 2016), which began observations in July 2014, also utilized *The Tractor* and the *WISE* component of the Legacy Surveys to target LRGs (Prakash et al. 2016) and QSOs (Myers et al. 2015). For these eBOSS targets, *The Tractor* was applied to obtain forced photometry based upon galaxy profiles measured by the SDSS imaging pipeline. Those profiles were convolved with the *WISE* PSF, and then a linear fit was performed on the full set of *WISE* imaging data. The result was a set of flux estimates for all SDSS objects, constructed so that the sum of flux-weighted profiles best matched the *WISE* images (Lang 2014; Lang et al. 2016b). DESI will make use of this same fitting approach, using the Legacy Surveys optical images in place of the SDSS images.

The Tractor catalogs include source positions, fluxes, shape parameters, and morphological quantities that can be used to discriminate extended sources from point-sources, together with errors on

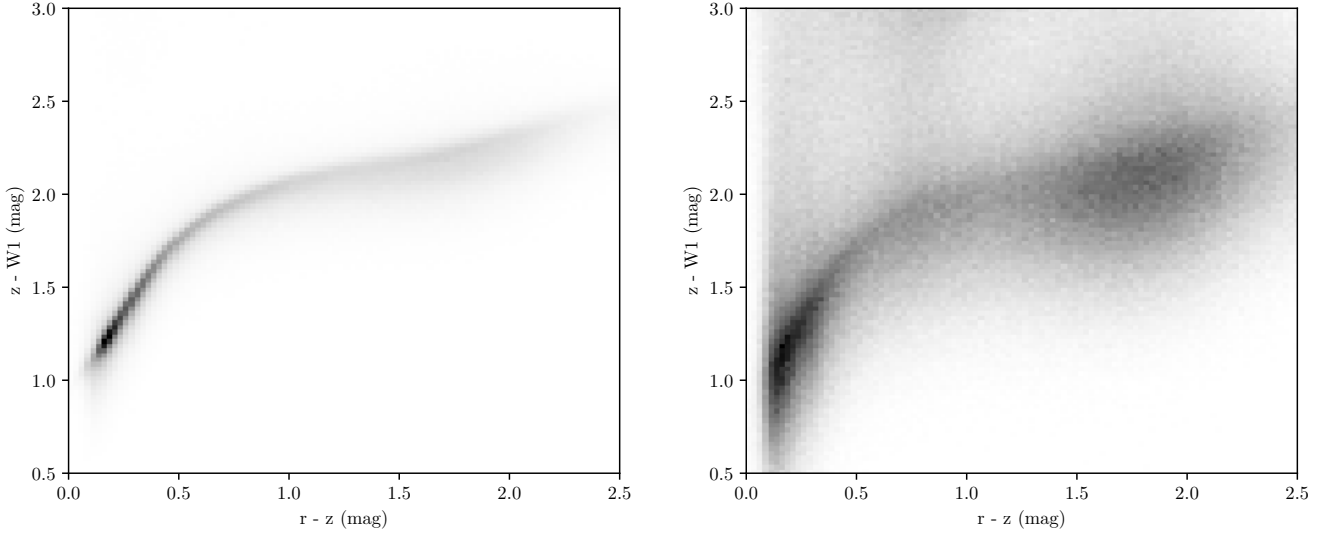


Figure 9. Forced photometry using *The Tractor*, contrasted with traditional “catalog-matching.” *Left:* Color-color diagram of catalog-matched PSF sources from the Legacy Surveys and AllWISE catalogs. *Right:* Color-color diagram of PSF sources from the Legacy Survey catalogs that have *no* matching object in the AllWISE catalog. Many of these will be sources that are well detected in the Legacy Surveys optical imaging, but below the detection threshold in the *WISE* imaging. We have applied a cut to show only *WISE* flux measurements above 3σ ; with this cut, we nearly double the number of sources with measured *WISE* fluxes. The distributions shown in both panels are similar, demonstrating that the forced photometry measurements of the faint mid-infrared sources make astrophysical sense, despite being noisier.

these quantities. *The Tractor* catalogs are vetted for DESI target selection using a series of image validation tests (as in e.g., Appendix C).

9. DATA RELEASES FROM THE LEGACY SURVEYS

The Legacy Surveys are being run as completely public projects. All raw optical imaging data are made available as soon as they are transferred from each telescope to the NOAO Science Archive¹⁵. The data transfer occurs within minutes for DECam and Mosaic3 data, and by the following morning for 90Prime data. Pipeline processed data are made public as soon as the reductions are completed, typically within a week of the observations. Finally, catalogs based on *The Tractor* and cross-matched data are released twice a year. All data (images, coadds, catalogs and supplementary material) are available at the NOAO Science Archive and through the Legacy Surveys portal hosted at NERSC¹⁶. All the code used for creating the catalogs is publicly available¹⁷. In addition, the BASS data are independently processed and released by the BASS team (e.g., see Zou et al. 2017b,c, for details).

Tables 3 and 6 show the observing schedule at the Blanco, Bok, and Mayall telescopes and our data release milestones. The data releases provide required deliverables such as object catalogs, depth maps, and co-added images, models, and residuals (see Table 7).

As of April 2018, the two most recent data releases are DR5 (containing all the DECaLS data obtained through 2017 May) and DR6 (containing all the MzLS and BASS data obtained through 2017 December 9 and 2017 June 25, respectively); see Table 6. Together, DR5+DR6 jointly cover

¹⁵ <http://archive.noao.edu>

¹⁶ <http://legacysurvey.org>

¹⁷ <https://github.com/legacysurvey/legacypipe> and <https://github.com/dstndstn/tractor>

nearly the entire DESI footprint and have significant overlap. The DR5 data release presents DECaLS data over $\approx 7,400 \text{ deg}^2$ in g -band, $8,000 \text{ deg}^2$ in r -band, and $10,200 \text{ deg}^2$ in z -band, with $6,800 \text{ deg}^2$ of coverage in all three bands. There are approximately 680 million unique sources in DR5 spread over 176,811 bricks. The DR6 data release presents MzLS+BASS data covering $\approx 4,400 \text{ deg}^2$ in g -band, $4,400 \text{ deg}^2$ in r -band, and $5,300 \text{ deg}^2$ in z -band, with $\approx 3,900 \text{ deg}^2$ with three-band coverage. There are approximately 310 million unique sources in DR6 spread over 92,287 bricks. Approximately 11,430 bricks overlap between DR5 and DR6 and contain more than 1000 objects each.

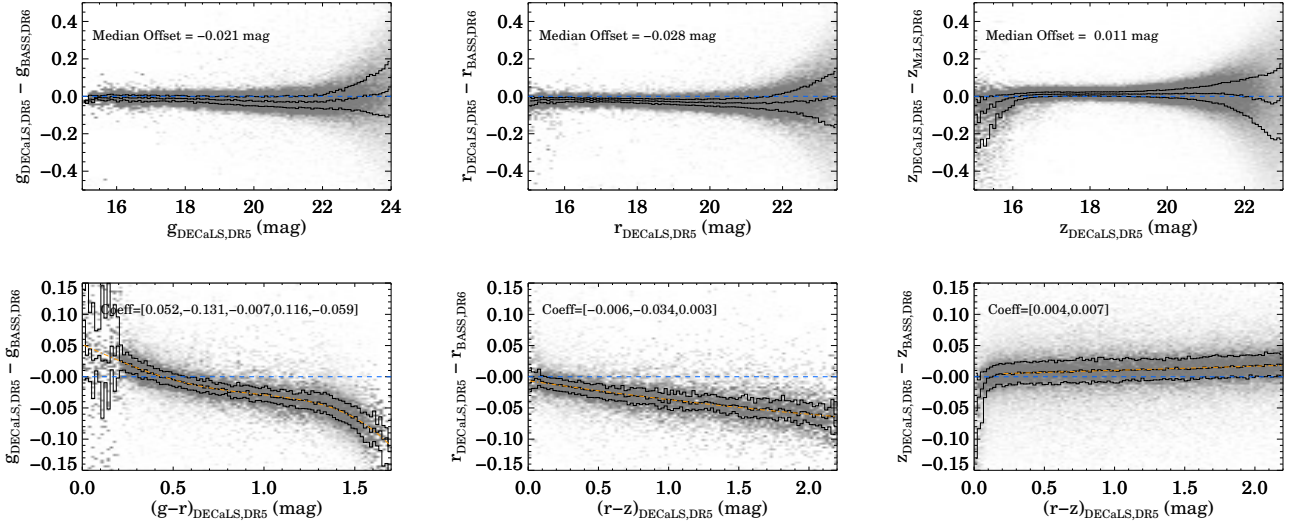


Figure 10. Comparison of grz photometry (top panels) and color transformations (bottom panels) for unresolved sources in common between the Legacy Surveys DR5 (DECaLS) and DR6 (BASS and MzLS) releases. In each panel the zero level is shown by a blue dashed line; the solid black lines represent the 25%, median and 75% quantiles, and the orange dot-dashed curve shows the polynomial fit. While there are significant color terms between the different telescope+camera combinations, the median differences are $< 30 \text{ mmag}$

Despite efforts to keep the filter bandpasses the same for the Kitt Peak and Cerro Tololo surveys, a direct comparison of the photometry for stellar sources observed by both sets yields the following color transformations (see Figure 10):

$$g_{\text{DR6,BASS}} = g_{\text{DR5,DECaLS}} - 0.052 + 0.131(g-r)_{\text{DR5}} + 0.007(g-r)_{\text{DR5}}^2 - 0.116(g-r)_{\text{DR5}}^3 + 0.059(g-r)_{\text{DR5}}^4 \quad (7)$$

$$r_{\text{DR6,BASS}} = r_{\text{DR5,DECaLS}} + 0.006 + 0.034(r-z)_{\text{DR5}} + 0.003(r-z)_{\text{DR5}}^2 \quad (8)$$

$$z_{\text{DR6,MzLS}} = z_{\text{DR5,DECaLS}} - 0.004 - 0.007(r-z)_{\text{DR5}} \quad (9)$$

These color transformations are determined using unresolved objects (i.e., type “PSF” in both catalogs) detected in the overlapping regions in both the DECaLS DR5 and BASS+MzLS DR6 catalogs. The polynomial least-squares fits were performed on samples restricted in magnitude and color: $[15, 22]$ and $0 < (g-r)_{\text{DR5}} < 1.7$ in g -band; and $[15, 21.5]$ and $0 < (r-z)_{\text{DR5}} < 2.2$ in r -band and z -band.

The median zero point offsets between DR5 and DR6 are:

$$< g_{\text{DR6,BASS}} - g_{\text{DR5,DECaLS}} > = 0.021 \text{ mag} \quad (10)$$

$$< r_{\text{DR6,BASS}} - r_{\text{DR5,DECaLS}} > = -0.028 \text{ mag} \quad (11)$$

$$< z_{\text{DR6,MzLS}} - z_{\text{DR5,DECaLS}} > = 0.011 \text{ mag} \quad (12)$$

These medians are computed for unresolved sources (i.e., type ‘PSF’ in both catalogs) with magnitudes and colors in the range [16,22] and $0 < (g-r) < 1.7$ for g -band; and [16,22] and $0 < (r-z) < 2.2$ in the r - and z -bands. Some portion (≈ 50 – 100 mmag) of these median offsets may be due to differences in the way the sky background is estimated in DR5 and DR6, and may disappear in future releases of the Legacy Surveys that incorporate a single, consistent sky-estimation algorithm. ++

Figure 11 shows the grz -band source number counts derived from DR5 and DR6 of the Legacy Surveys. Figure 12 shows the grz -band depths for the DR5 and DR6 data. The DR6 imaging (from BASS and MzLS) is shallower than the DR5 imaging (from DECaLS), but still satisfies the DESI target selection requirements.

Figure 14 shows the distributions, in $grzW1$ color-color planes, of sources from the Legacy Surveys DR5 differentiated by their morphological type. Sources best fit by PSF models are dominated by stars (as exemplified by the clearly visible stellar locus), but also contain compact galaxies and QSOs. The sources best fit by spatially extended models (EXP: exponential disks; and DEV: de Vaucouleurs $r^{1/4}$ profiles) trace the galaxy locus with minimal contamination from stars (since the star-galaxy separation is limited by the ground-based seeing).

Figure 15 shows cutouts of a wide variety of astronomical sources imaged by the Legacy Surveys, to demonstrate the depth and image quality of the surveys. The large time baseline between the Legacy Surveys and SDSS also enable the detection of faint transients and the measurement of proper motions for faint stars (Figure 16 shows an example). The sensitivity of the Legacy Surveys data to low surface brightness structures has been exploited in the new version of Galaxy Zoo (<https://blog.galaxyzoo.org/tag/decals/>) and for finding faint tidal features associated with galaxies (e.g., Hood et al. 2018). In addition, the depth of the Legacy Surveys data has resulted in their use for selecting emission-line galaxy (DECaLS component; Raichoor et al. 2017) and QSO targets (*WISE* component Myers et al. 2015) for the SDSS-IV/eBOSS spectroscopic survey.

All observations for the MzLS completed on 2018 February 12. Observing for BASS will continue through 2018 July. Observing for DECaLS is estimated to continue until 2019 January. The goal of the Legacy Surveys is to consolidate the data from all the subsidiary surveys into a final data release by 2019 June.

10. SUMMARY

We have begun three wide-area optical imaging surveys, that will cover a total area of $14,000 \text{ deg}^2$ in two contiguous portions and in three filters. These surveys are designed to provide targets for the DESI project, which will begin spectroscopic observations in 2019. The surveys include optical imaging data in three bands (g -, r -, and z -band) from three ground-based telescopes (CTIO Blanco, KPNO Mayall and Steward Bok 90”) and will reach approximate 5σ depths of $g=24.0$, $r=23.4$ and $z=22.5$ AB mag for faint galaxies. In addition, the data releases will contain mid-infrared photometry based on new, multi-epoch stacks of imaging data from the *WISE* satellite created by the unWISE project. The three surveys are the Dark Energy Camera Legacy Survey (DECaLS), the Mayall z -

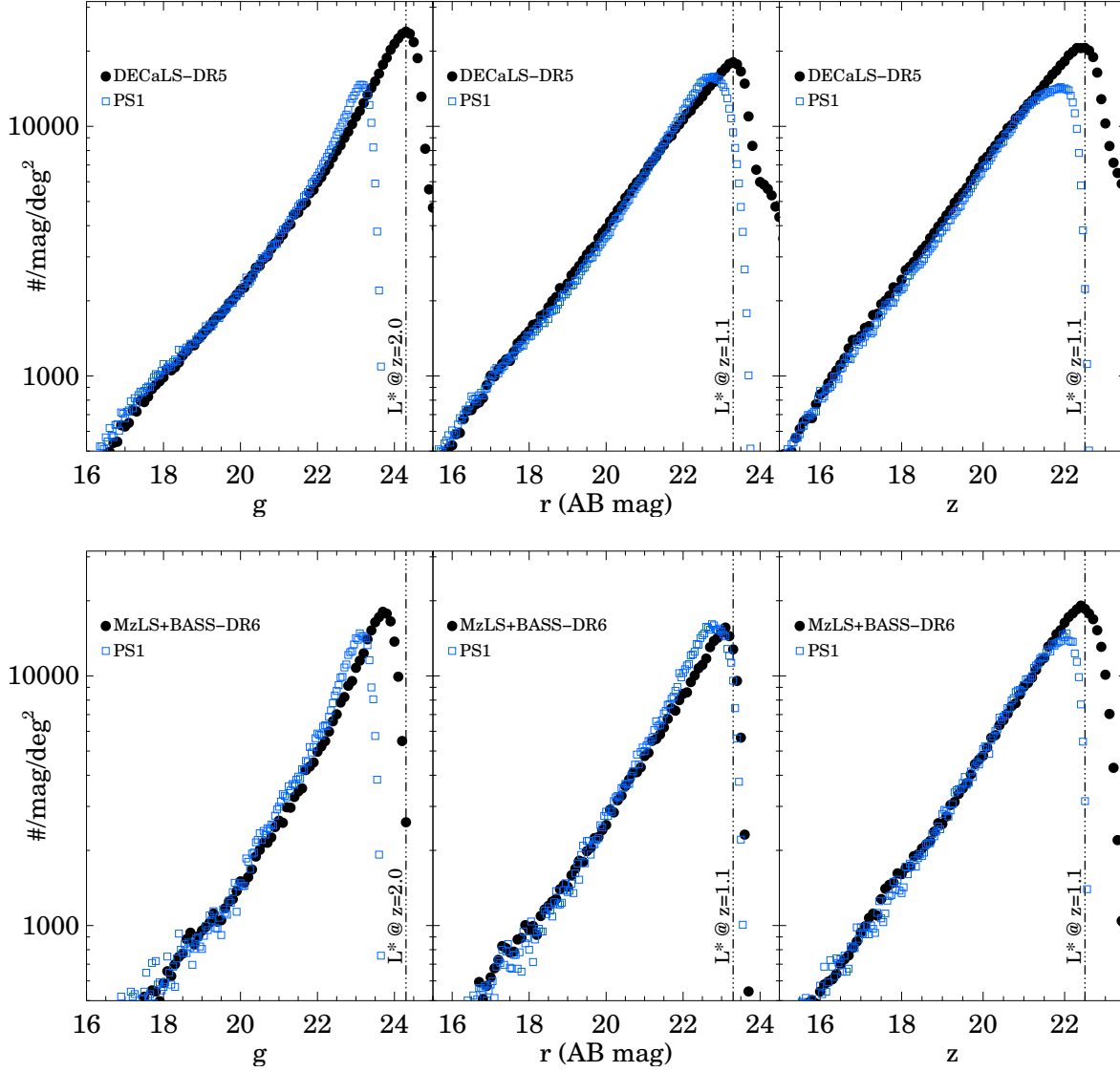


Figure 11. Number counts of all detected sources measured from the Legacy Surveys DR5 and DR6 data releases compared with source counts from the PS1 survey. The DR5 number counts are measured in an $\approx 20.4 \text{ deg}^2$ region centered on $(\text{RA}, \text{DEC}) = (243.311^\circ, 9.387^\circ)$. The DR6 number counts are measured in an $\approx 3.3 \text{ deg}^2$ region centered on $(245.55^\circ, 43.27^\circ)$. All the data shown are for sources detected at signal-to-noise ratios ≥ 5 , and the PS1 sources are required to be detected in at least two of the grz bands in order to exclude spurious sources.

band Legacy Survey (MzLS) and the Beijing-Arizona Sky Survey (BASS); these surveys are jointly referred to as the Legacy Surveys.

We have implemented a dynamic observing strategy for all surveys, where observing conditions are monitored in near-real time and exposure times are modified on-the-fly to ensure that each individual observation reaches the required depth and that the ground-based surveys produce datasets that are as uniform as possible. The data are pipeline processed and catalogs are generated from the imaging data using an inference-based forward modeling approach known as *The Tractor*.

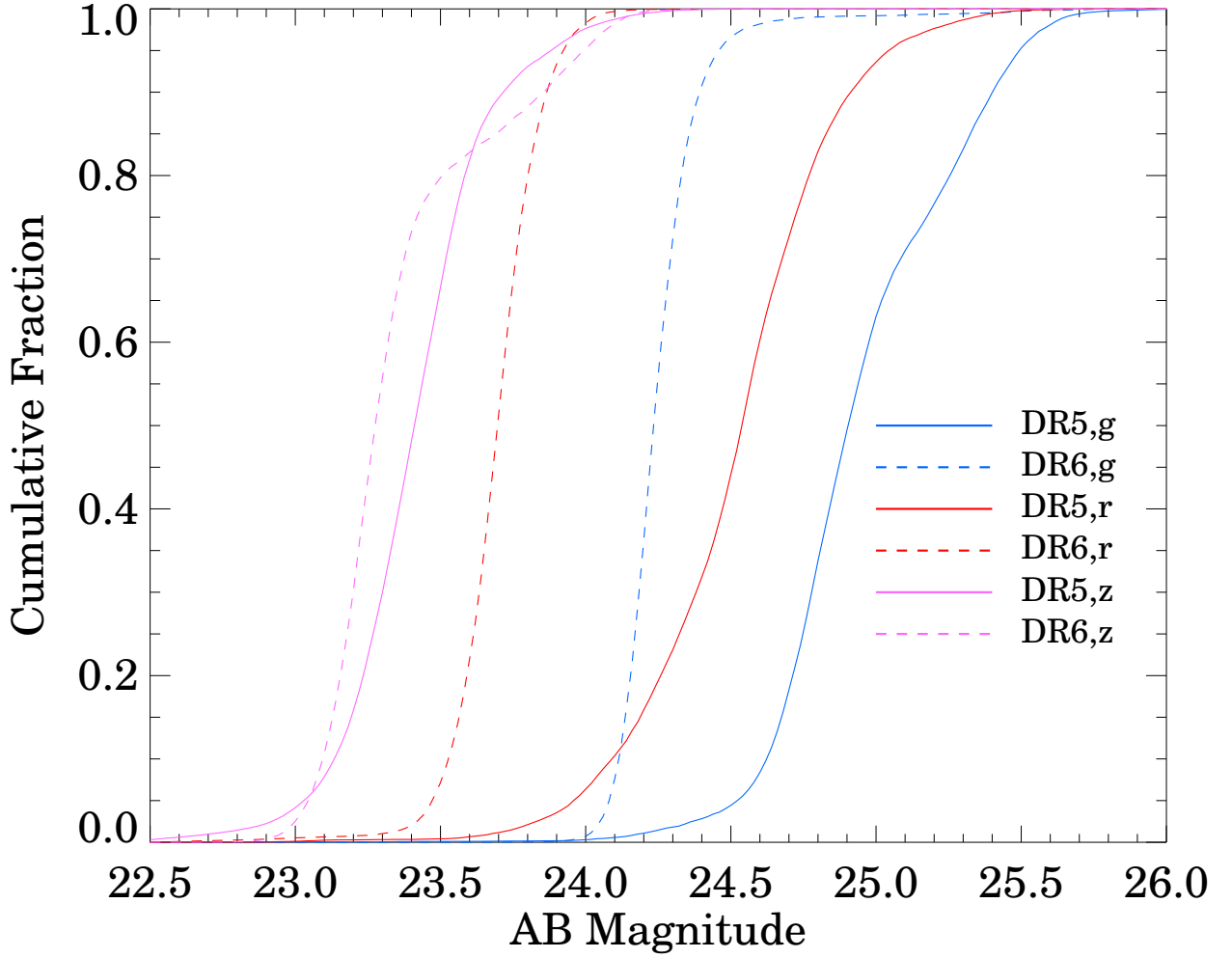


Figure 12. The *grz* 5σ point-source depths in ≥ 3 -pass data in the Legacy Surveys DR5 (data from DECaLS survey) and DR6 (data from BASS+MzLS surveys) releases.

All the imaging data, source catalogs, and code from the Legacy Surveys are publicly available: the raw and pipeline-processed optical imaging data are made public as soon as they are available in the NOAO Archive and catalogs from the project are released approximately twice each year. There have been 6 data releases thus far, which are described in detail in other papers. The imaging data are accessible from the Legacy Surveys website¹⁸ and the NOAO Science Archive¹⁹. An image viewer is provided at the Legacy Surveys website that allows the user to examine the data, *The Tractor* models, and other supplementary data. A resource at the NOAO DataLab provides access to the catalogs through SQL queries or a Jupyter notebook interface²⁰.

The Legacy Surveys are currently in progress. We anticipate completing the surveys before the start of DESI spectroscopic observations in 2019.

¹⁸ <http://legacysurvey.org>, served by NERSC

¹⁹ <http://archive.noao.edu>

²⁰ see <https://datalab.noao.edu/decals/lis.php> for details

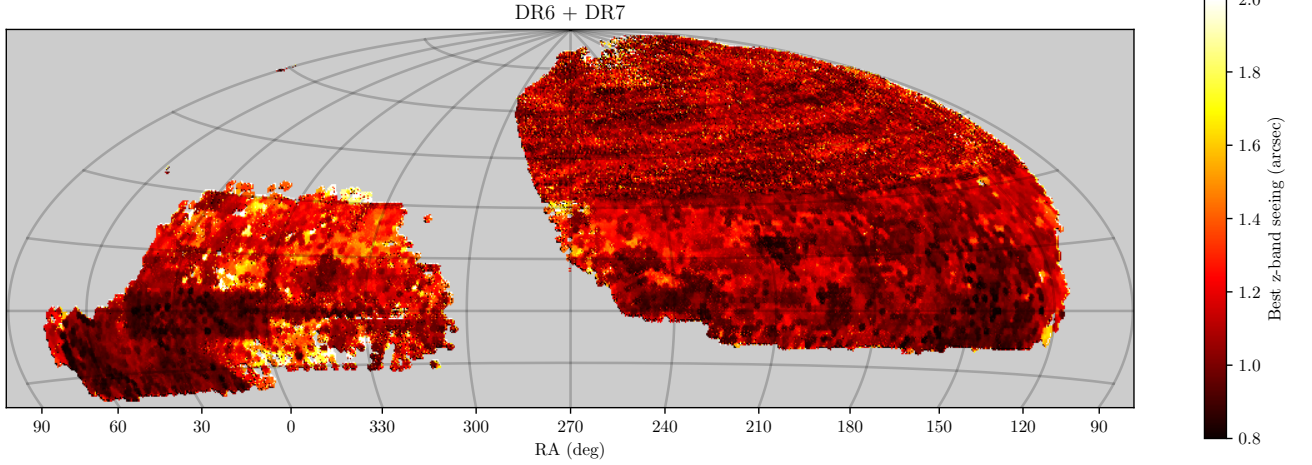


Figure 13. The spatial distribution (at 0.5° resolution) of image quality represented by the best-seeing z -band data in the Legacy Surveys DR5 and DR6 releases. The *The Tractor* source modeling is dependent on the data with the best delivered image quality at any given location. The DECaLS survey (covering the region south of $\delta \sim +30^\circ$) is still incomplete, as reflected by the variable image quality in much of this region. The DR6 release of MzLS also did not include the full MzLS dataset.

Table 6. Data Releases for the Legacy Surveys

DR	Release Date	Surveys	W1/W2 Depth (yr)	Image/Catalog Data Volume	Number of Sources
1	2015 May	DECaLS	1	15TB/238GB	140 million
2	2016 January	DECaLS	2	33TB/301GB	260 million
3	2016 September	DECaLS	2	57TB/663GB	478 million
4	2017 June	BASS+MzLS	3	30TB/256GB	183 million
5	2016 October	DECaLS	3	18TB/969GB	680 million
6	2018 February	BASS+MzLS	4	9TB/449GB	310 million
7	2018 July	DECaLS	4		
8	2019 January	All	5		
9	2019 June	All	5		

This paper presents observations obtained at Cerro Tololo Inter-American Observatory, National Optical Astronomy Observatory (NOAO Prop. ID: 2014B-0404; co-PIs: D. J. Schlegel and A. Dey), which is operated by the Association of Universities for Research in Astronomy (AURA) under a cooperative agreement with the National Science Foundation. This paper also includes DECam observations obtained as part of other projects, namely the Dark Energy Survey (DES, NOAO Prop. ID: 2012B-0001); and 2012B-0003, 2012B-0416, 2012B-0506, 2012B-0569, 2012B-0617, 2012B-0621, 2012B-0624, 2012B-0625, 2012B-3003, 2012B-3011, 2012B-3012, 2012B-3016, 2012B-9993, 2012B-9999, 2013A-0327, 2013A-0360, 2013A-0386, 2013A-0400, 2013A-0455, 2013A-0529, 2013A-0609, 2013A-0610, 2013A-0611, 2013A-0613, 2013A-0614, 2013A-0618, 2013A-0704, 2013A-0716, 2013A-0717, 2013A-0719, 2013A-0723, 2013A-0724, 2013A-0737, 2013A-0739, 2013A-0741, 2013A-9999, 2013B-0325, 2013B-0438, 2013B-0440, 2013B-0453, 2013B-0502, 2013B-0531, 2013B-0612, 2013B-

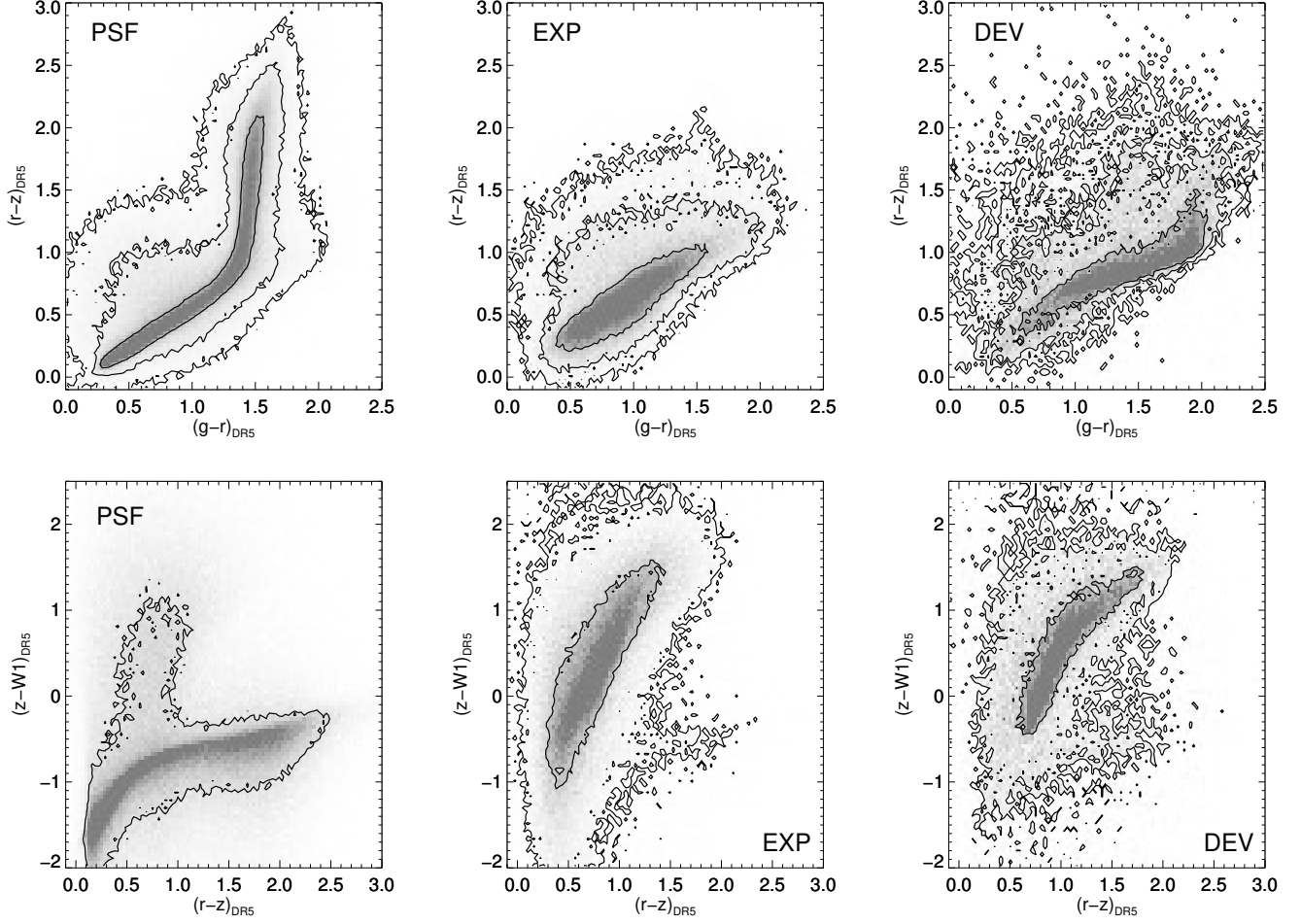


Figure 14. The distribution, in the $g-r-z-W1$ color-color planes, of three of the morphological model types from DR5. The PSF type (left panels) corresponds to unresolved sources, which include stars, distant QSOs and some unresolved galaxies. The EXP and DEV types (middle and right panels respectively) are sources that are best fit by exponential disk or de Vaucouleurs $r^{1/4}$ light profiles. All colors are in units of AB magnitudes.

Table 7. Data Products from the Legacy Surveys

Data Product Name	Type	Description
image	image	Coadded image per band
invvar	image	Inverse-variance map per band
model	image	Coadded model image per band
chi2	image	Coadded chi-squared image $((\text{image-model})^2 \times \text{invvar})$ per band
depth	image	PSF depth (as inverse-variance) per band
galdepth	image	Fiducial galaxy depth (as inverse-variance) per band
nexp	image	Number of exposures per band
tractor	catalog	Tractor catalog of measured sources, per brick

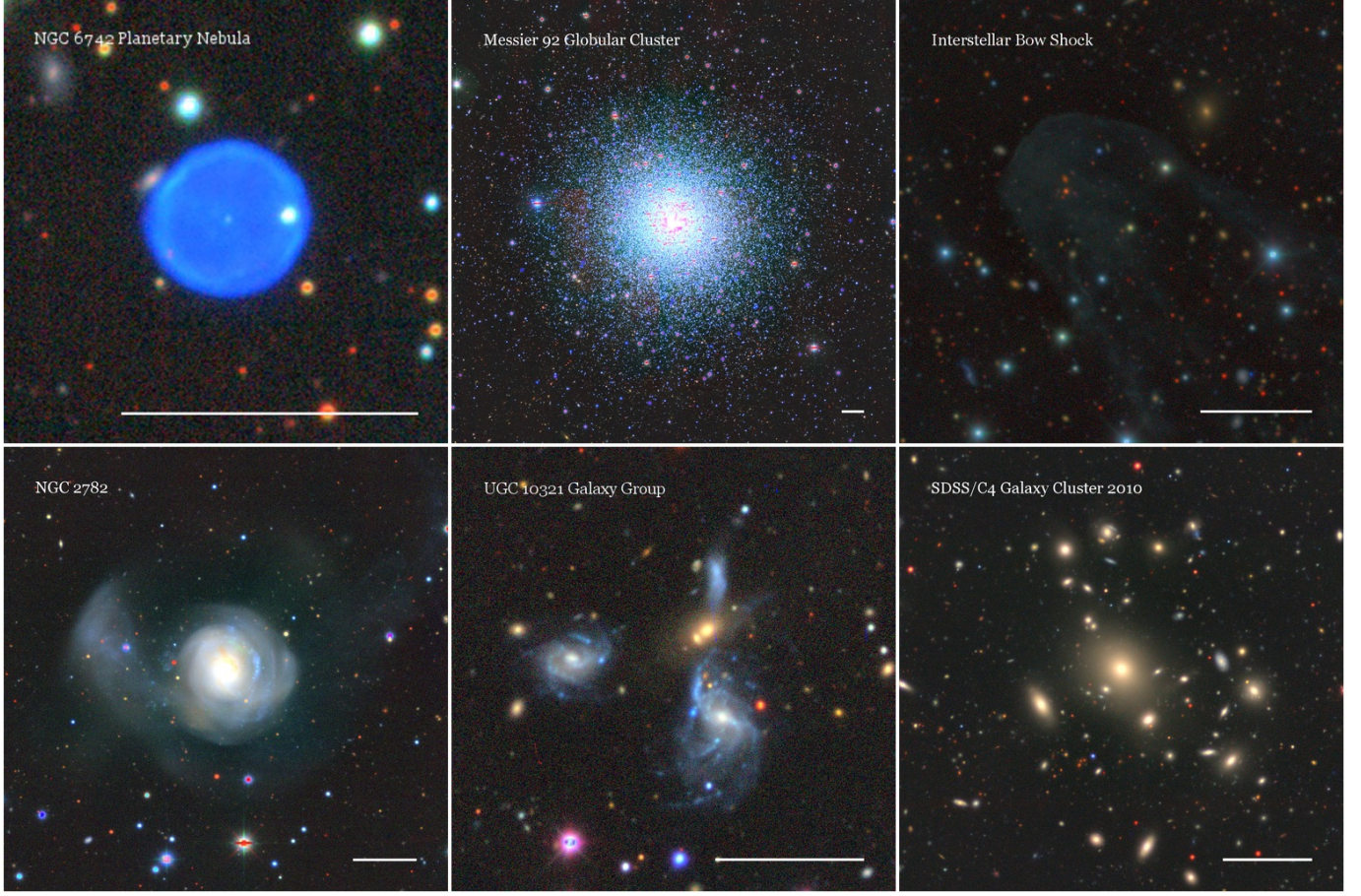


Figure 15. A gallery of image cutouts from the DR6 Legacy Surveys data illustrating the variety of astronomical objects covered by the surveys and highlighting the capability of the surveys to image low surface brightness features. The horizontal bar in the bottom right corner of each panel represents an angular size scale of $1'$. In all images, north is up and east is to the left. More examples are shown in the DR5 and DR6 online image galleries.

0613, 2013B-0615, 2013B-0616, 2013B-0617, 2014A-0073, 2014A-0191, 2014A-0239, 2014A-0255, 2014A-0256, 2014A-0270, 2014A-0306, 2014A-0313, 2014A-0321, 2014A-0327, 2014A-0339, 2014A-0348, 2014A-0386, 2014A-0390, 2014A-0412, 2014A-0415, 2014A-0429, 2014A-0496, 2014A-0608, 2014A-0610, 2014A-0611, 2014A-0613, 2014A-0620, 2014A-0621, 2014A-0622, 2014A-0623, 2014A-0624, 2014A-0632, 2014A-0640, 2014B-0146, 2014B-0244, 2014B-0608, 2014B-0610, 2014B-0614, 2015B-0187.

DECaLS used data obtained with the Dark Energy Camera (DECam), which was constructed by the Dark Energy Survey (DES) collaboration. Funding for the DES Projects has been provided by the U.S. Department of Energy, the U.S. National Science Foundation, the Ministry of Science and Education of Spain, the Science and Technology Facilities Council of the United Kingdom, the Higher Education Funding Council for England, the National Center for Supercomputing Applications at the University of Illinois at Urbana-Champaign, the Kavli Institute of Cosmological Physics at the University of Chicago, Center for Cosmology and Astro-Particle Physics at the Ohio State University, the Mitchell Institute for Fundamental Physics and Astronomy at Texas A&M University, Financiadora

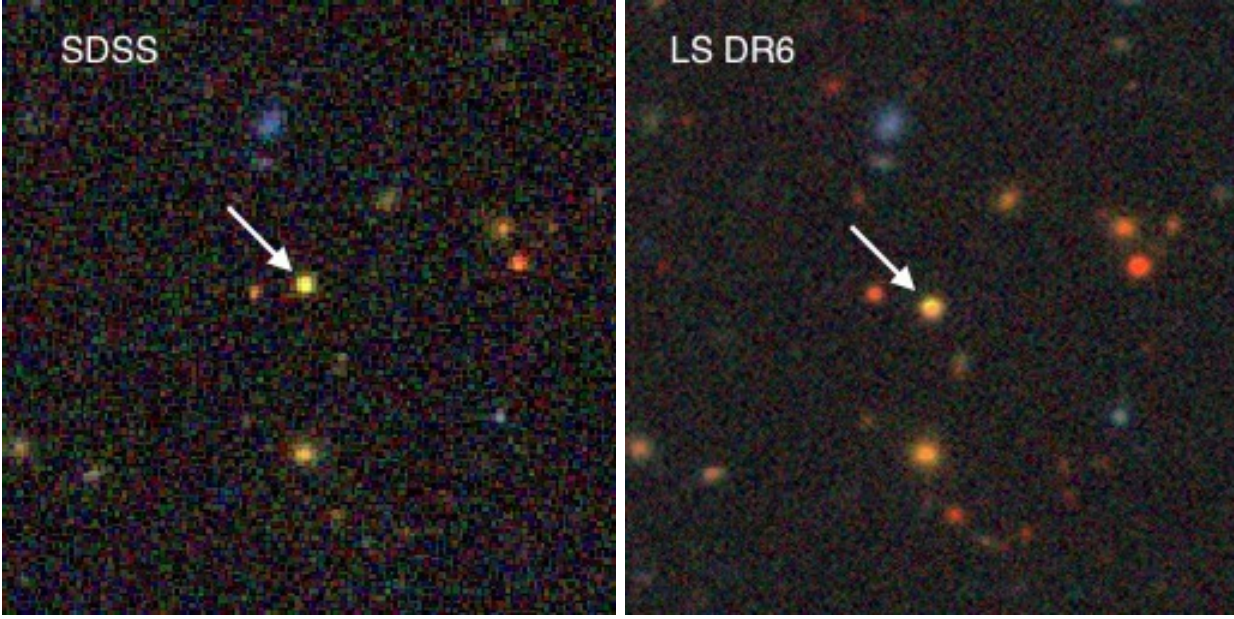


Figure 16. A new high proper motion star at $(RA, DEC) = (223.7678^\circ, +33.7066^\circ)$ discovered serendipitously in DR6 of the Legacy Surveys. The left and right panels show $\approx 67 \times 67''$ cutouts of the SDSS and DR6 images, respectively, extracted from the Legacy Surveys’ image viewer; north is up and east is to the left. The $g = 21.2$ AB mag M0V star (classified based on an SDSS spectrum) is moving at $\approx 0.2''$ per year. The large time baseline (≈ 14 years) between the SDSS and Legacy Surveys data will enable proper motion measurements for stars fainter than the Gaia catalog limits.

de Estudos e Projetos, Fundação Carlos Chagas Filho de Amparo, Financiadora de Estudos e Projetos, Fundação Carlos Chagas Filho de Amparo à Pesquisa do Estado do Rio de Janeiro, Conselho Nacional de Desenvolvimento Científico e Tecnológico and the Ministério da Ciência, Tecnologia e Inovação, the Deutsche Forschungsgemeinschaft and the Collaborating Institutions in the Dark Energy Survey. The Collaborating Institutions are Argonne National Laboratory, the University of California at Santa Cruz, the University of Cambridge, Centro de Investigaciones Energéticas, Medioambientales y Tecnológicas-Madrid, the University of Chicago, University College London, the DES-Brazil Consortium, the University of Edinburgh, the Eidgenössische Technische Hochschule (ETH) Zürich, Fermi National Accelerator Laboratory, the University of Illinois at Urbana-Champaign, the Institut de Ciències de l’Espai (IEEC/CSIC), the Institut de Física d’Altes Energies, Lawrence Berkeley National Laboratory, the Ludwig-Maximilians Universität München and the associated Excellence Cluster Universe, the University of Michigan, the National Optical Astronomy Observatory, the University of Nottingham, the Ohio State University, the University of Pennsylvania, the University of Portsmouth, SLAC National Accelerator Laboratory, Stanford University, the University of Sussex, and Texas A&M University.

The Mayall z -band Legacy Survey (MzLS; NOAO Prop. ID # 2016A-0453; PI: A. Dey) uses observations made with the Mosaic3 camera at the Mayall 4m telescope at Kitt Peak National Observatory, National Optical Astronomy Observatory, which is operated by the Association of Universities for Research in Astronomy (AURA) under cooperative agreement with the National Science Foundation. The authors are honored to be permitted to conduct astronomical research on Iolkam Du’ag (Kitt Peak), a mountain with particular significance to the Tohono O’odham.

The Beijing-Arizona Sky Survey (BASS; NOAO Proposal ID # 2015A-0801; PIs: Zhou Xu and Xiaohui Fan) is a key project of the Telescope Access Program (TAP), which has been funded by the National Astronomical Observatories of China, the Chinese Academy of Sciences (the Strategic Priority Research Program “The Emergence of Cosmological Structures” Grant # XDB09000000), and the Special Fund for Astronomy from the Ministry of Finance. The BASS is also supported by the External Cooperation Program of Chinese Academy of Sciences (Grant # 114A11KYSB20160057), and Chinese National Natural Science Foundation (Grant # 11433005). The Bok Telescope is located on Kitt Peak and operated by Steward Observatory, University of Arizona.

The Legacy Surveys imaging of the DESI footprint is supported by the Director, Office of Science, Office of High Energy Physics of the U.S. Department of Energy under Contract No. DE-AC02-05CH11231, by the National Energy Research Scientific Computing Center, a DOE Office of Science User Facility under the same contract; and by the U.S. National Science Foundation, Division of Astronomical Sciences under Contract No. AST-0950945 to NOAO. Travel and other support for the DECaLS and MzLS projects is provided by the National Optical Astronomy Observatory, the Lawrence Berkeley National Laboratory, and the DESI Project.

This publication makes use of data from the Pan-STARRS1 Surveys (PS1) and the PS1 public science archive, which have been made possible through contributions by the Institute for Astronomy, the University of Hawaii, the Pan-STARRS Project Office, the Max-Planck Society and its participating institutes, the Max Planck Institute for Astronomy, Heidelberg and the Max Planck Institute for Extraterrestrial Physics, Garching, The Johns Hopkins University, Durham University, the University of Edinburgh, the Queen’s University Belfast, the Harvard-Smithsonian Center for Astrophysics, the Las Cumbres Observatory Global Telescope Network Incorporated, the National Central University of Taiwan, the Space Telescope Science Institute, the National Aeronautics and Space Administration under Grant No. NNX08AR22G issued through the Planetary Science Division of the NASA Science Mission Directorate, the National Science Foundation Grant No. AST-1238877, the University of Maryland, Eotvos Lorand University (ELTE), the Los Alamos National Laboratory, and the Gordon and Betty Moore Foundation.

This work has made use of data from the European Space Agency (ESA) mission *Gaia* (<https://www.cosmos.esa.int/gaia>), processed by the *Gaia* Data Processing and Analysis Consortium (DPAC, <https://www.cosmos.esa.int/web/gaia/dpac/consortium>). Funding for the DPAC has been provided by national institutions, in particular the institutions participating in the *Gaia* Multilateral Agreement.

This publication makes use of data products from the Wide-field Infrared Survey Explorer (and its successor, the Near-Earth Object Wide-field Infrared Survey Explorer), which is a joint project of the University of California, Los Angeles, and the Jet Propulsion Laboratory/California Institute of Technology, funded by the National Aeronautics and Space Administration.

This research used resources of the National Energy Research Scientific Computing Center, a DOE Office of Science User Facility supported by the Office of Science of the U.S. Department of Energy under Contract No. DE-AC02-05CH11231.

The research leading to these results has received funding from the European Research Council under the European Union’s Seventh Framework Programme (FP/2007-2013) / ERC Grant Agreement n. 320964 (WDTracer).

APPENDIX

A. DESI IMAGING REQUIREMENTS

Imaging data from the Legacy Surveys will be used to select targets for DESI. In this Appendix, we describe the basic requirements that the DESI project’s main cosmological survey imposes on imaging. There are five target classes for the DESI dark energy experiment: (1) Bright Galaxy Sample (BGS); (2) Luminous Red Galaxies (LRGs); (3) Emission Line Galaxies (ELGs); (4) quasars (QSOs) at $z < 2.1$; and (5) quasars at $z > 2.1$ for the measurement of the Lyman-alpha forest. The imaging surveys will also be used to select secondary targets such as other interesting object classes (rare objects, Galactic stars, etc.), standard stars for spectrophotometric calibration, and locations for blank sky fibers.

In 2013, the DESI Project concluded that a three-band $g/r/z$ optical imaging program complemented by *WISE* W1 and W2 photometry would be sufficient to select all target classes required for the DESI cosmology program. One optical band is sufficient to select the BGS, which is defined as a simple magnitude-limited sample. Two optical bands are necessary to select LRGs and quasars, as the *WISE* W1 infrared band provides adequate color information to clearly separate these targets from stars and other galaxies. Three optical bands are necessary to efficiently select the ELGs, as these galaxies are not well-detected at the depth of the *WISE* data. Other imaging data (e.g., u -band) may be used to further refine the selection of the high-redshift QSOs, which is the one target class that is not required (by DESI) to have a uniform selection if used for Lyman-alpha forest maps.

The requirements that DESI targeting imposes on the optical imaging are:

1. **Imaging will be in three optical bands to a depth of at least $g = 24.0$, $r = 23.4$ and $z = 22.5$.** The depths are defined as the optimal-extraction (forced-photometry) depths for a galaxy near the depth limits of DESI, where that galaxy is defined to be an exponential profile with a half-light radius of $r_{\text{half}} = 0.45$ arcsec. For such a profile, the effective number of pixels is well-approximated by $N_{\text{eff}} = [(4\pi\sigma^2)^{(1/p)} + (8.91r_{\text{half}}^2)^{(1/p)}]^p$, where σ is the standard deviation for a Gaussian fit to the seeing, r_{half} is the half-light radius for an exponential-profile galaxy, and $p = 1.15$. In addition to the optical imaging, 4 years of *WISE* data in the W1 and W2 bands are assumed.
2. **Imaging will cover at least 14,000 deg² of the DESI footprint.** This footprint is described in § 3.
3. **The fill factor will be at least 90%.** The areas with coverage to full depth in all 3 bands should exceed 90% of the footprint. The science loss is approximately proportional to this fractional loss of area.
4. **z -band image quality will be smaller than 1.5 arcsec FWHM.** Many of the DESI galaxy targets appear small (less than 1 arcsec) and are near the limit at which they can be resolved as extended sources rather than point sources. Because of this, a morphological separation between extended sources and point sources will not be required for DESI galaxy targets. The

primary driver for reasonably good image quality is to minimize blending between targets and other sources on the sky, especially in regions of high stellar density, such as near the Galactic plane. Reasonable image quality in at least one band will allow the identification of otherwise blended objects and the optimal extraction of their photometry in all bands. All of the DESI targets will be detected in z -band, which is expected to have the best image quality, therefore an image quality requirement is specified in that one band.

5. **No regions larger than 3 deg in diameter will be covered by only nonphotometric observations.** Photometric observations are defined as those obtained during nights demonstrated to have photometricity errors of 1% RMS in g -band and r -band, or 2% RMS in z -band. Small regions, especially in CCD gaps on the imager focal planes, may be filled in with non-photometric data and calibrated to neighboring, photometric data.
6. **The random errors in astrometry will be less than 95 mas RMS, and the systematic errors will be less than 30 mas.** Astrometric errors impact the effective throughput of the DESI instrument for the spectroscopic survey. The systematics errors in the astrometry will be well-controlled by tying individual CCD images to Gaia (Gaia Collaboration et al. 2016b). The astrometric positions can take advantage of the signal in all filters.

An inference modeling approach will be used for measuring the photometry in all bands from the optical and *WISE* imaging data. The DESI requirements for the imaging *reductions* are:

1. **The model photometry will use the same model in all bands.** The model photometry uses the same model in all bands to minimize systematic errors in the flux ratios (i.e., colors) of galaxies, which is critical for all target selection algorithms.
2. **Systematic errors due to PSF mis-estimation will be controlled to better than 1%.**
3. **Systematic errors due to galaxy model mis-estimation will be controlled to better than 1%.** A simple χ^2 fit would suffer from biases in the galaxy photometry due to the models not matching the actual morphology of individual galaxies, and this would be S/N-dependent.
4. **Depth maps will be computed in each band at all locations.** The effective depth will be computed as a map for each filter. This is a function of the sky brightness, image quality and sky transparency of all of the contributing images. In detail on small scales, it would include the features seen from bad columns on the CCD and increased noise near other sources on the sky.
5. **The ability will be provided to Monte Carlo simulated objects through the imaging pipeline.** This requirement implies access to all of the calibrated image frames, the versioned code used to construct the final targeting catalogs, and the ability to run this code. This Monte Carlo ability will be used to map the effects of bright stars and other source contamination problems, which can both produce spurious targets and remove actual targets by blending them with other sources.

B. TRANSFORMATIONS FROM SDSS TO LEGACY SURVEYS PHOTOMETRY

We compared the SDSS and Legacy Surveys photometry in two regions using the “sweeps” files which contain matched SDSS and Legacy Survey sources and are included as part of the DR5 and

DR6 Legacy Survey releases. For the SDSS-DR5 comparison, we used the region $160^\circ \leq \text{RA} \leq 170^\circ$ and $2.0^\circ \leq \text{DEC} \leq 2.5^\circ$; for the SDSS-DR6 comparison, we used the region $230^\circ \leq \text{RA} \leq 240^\circ$ and $2.0^\circ \leq \text{DEC} \leq 2.5^\circ$. The photometric transformations were then computed by fitting polynomials to the SDSS-Legacy Survey magnitude differences in the g , r and z bands as a function of the SDSS $(g-i)$ color. The fits were done in the color range $-0.25 \leq (g-i)_{\text{SDSS}} \leq 3.5$ and restricted to bright stars (i.e., $i \leq 19$). The resulting transformations are:

$$g_{\text{DR5,DECaLS}} \approx g_{\text{SDSS}} + 0.0258 - 0.108(g-i)_{\text{SDSS}} + 0.0258(g-i)_{\text{SDSS}}^2 - 0.0057(g-i)_{\text{SDSS}}^3 \quad (\text{B1})$$

$$r_{\text{DR5,DECaLS}} \approx r_{\text{SDSS}} - 0.0112 - 0.0897(g-i)_{\text{SDSS}} + 0.0300(g-i)_{\text{SDSS}}^2 - 0.0094(g-i)_{\text{SDSS}}^3 \quad (\text{B2})$$

$$z_{\text{DR5,DECaLS}} \approx z_{\text{SDSS}} - 0.0285 - 0.0221(g-i)_{\text{SDSS}} + 0.0030(g-i)_{\text{SDSS}}^2 - 0.0013(g-i)_{\text{SDSS}}^3 \quad (\text{B3})$$

$$g_{\text{DR6,BASS}} \approx g_{\text{SDSS}} - 0.0125 - 0.0535(g-i)_{\text{SDSS}} + 0.0162(g-i)_{\text{SDSS}}^2 - 0.0047(g-i)_{\text{SDSS}}^3 \quad (\text{B4})$$

$$r_{\text{DR6,BASS}} \approx r_{\text{SDSS}} - 0.0215 - 0.0683(g-i)_{\text{SDSS}} + 0.0265(g-i)_{\text{SDSS}}^2 - 0.0084(g-i)_{\text{SDSS}}^3 \quad (\text{B5})$$

$$z_{\text{DR6,MzLS}} \approx z_{\text{SDSS}} - 0.0293 - 0.0387(g-i)_{\text{SDSS}} + 0.0123(g-i)_{\text{SDSS}}^2 - 0.0034(g-i)_{\text{SDSS}}^3 \quad (\text{B6})$$

The typical root-mean-square photometric scatter around these transformation relations is $\sigma \approx 30$ mmag.

C. COMPARING SUBARU HYPER-SUPRIME CAMERA AND LEGACY SURVEYS DATA

We have compared data from DR1 of the Subaru Hyper-SuprimeCam (HSC) surveys (Aihara et al. 2018)²¹ with data from the Legacy Surveys in two regions: (1) $244.5^\circ \leq \text{RA} \leq 246.5^\circ$, $43.0^\circ \leq \text{DEC} \leq 44.0^\circ$; and (2) $31.5^\circ \leq \text{RA} \leq 36^\circ$, $-6^\circ \leq \text{DEC} \leq -4.5^\circ$. The first region corresponds to the ‘‘HECTOMAP’’ region in the HSC survey, and is covered by the Legacy Surveys DR6 data. The second region corresponds to the XMM-LSS region in the HSC survey, and is covered by the Legacy Surveys DR5 data. We compared the HSC photometry to the DR5 and DR6 data and derived the following transformations:

$$g_{\text{DR5,DECaLS}} \approx g_{\text{HSC}} + 0.0146 - 0.0146(g-r)_{\text{HSC}} \quad (\text{C7})$$

$$r_{\text{DR5,DECaLS}} \approx r_{\text{HSC}} - 0.0147 - 0.1714(r-z)_{\text{HSC}} + 0.0704(r-z)_{\text{HSC}}^2 - 0.0162(r-z)_{\text{HSC}}^3 \quad (\text{C8})$$

$$z_{\text{DR5,DECaLS}} \approx z_{\text{HSC}} - 0.0296 - 0.0420(r-z)_{\text{HSC}} + 0.0024(r-z)_{\text{HSC}}^2 \quad (\text{C9})$$

$$g_{\text{DR6,BASS}} \approx g_{\text{HSC}} - 0.0121 + 0.0383(g-r)_{\text{HSC}} \quad (\text{C10})$$

$$r_{\text{DR6,BASS}} \approx r_{\text{HSC}} - 0.1402(r-z)_{\text{HSC}} + 0.0681(r-z)_{\text{HSC}}^2 - 0.0180(r-z)_{\text{HSC}}^3 \quad (\text{C11})$$

$$z_{\text{DR6,MzLS}} \approx z_{\text{HSC}} - 0.0418 - 0.0433(r-z)_{\text{HSC}} - 0.0007(r-z)_{\text{HSC}}^2 \quad (\text{C12})$$

The 50% completeness limits (measured relative to HSC) in $[g, r, z]$ are $[25.26, 24.84, 24.29]$ AB mag in DR5 and $[24.535, 24.235, 23.336]$ AB mag in DR6, respectively. Of the 95,241 DR6 sources in region (1), 3,506 (3.7%) have no matches in the HSC catalog. 713 of these are bright sources ($g \leq 17, r \leq 18, z \leq 17$) and are likely saturated in the HSC data; 1,431 are fainter than the 80% completeness limits. We examined 100 DR6 sources with magnitudes $20 < g < 22$ that are missing in the HSC catalogs and found that 83 are fake sources (33 due to particle events; 22 due to increased noise in, e.g., regions near CCD edges; 28 are fake sources created by *The Tractor* in the extended halos of bright (typically saturated) stars or galaxies; and the remaining are real sources that have

²¹ See <http://hsc.mtk.nao.ac.jp/ssp/survey/>

been split into multiple sources due to their complexity, or mis-centered (due to low signal-to-noise data) in the DR6 catalog, or are low surface brightness sources not present in the HSC catalog. Despite these issues, the DR6 catalog reliability is higher than PS1 at faint magnitudes.

REFERENCES

- Abareshi, B., Marshall, R., Gott, S., et al. 2016, in Proc. SPIE, Vol. 9913, Software and Cyberinfrastructure for Astronomy IV, 99131O
- Abazajian, K. N., Adelmann-McCarthy, J. K., Agüeros, M. A., et al. 2009, ApJS, 182, 543
- Aihara, H., Armstrong, R., Bickerton, S., et al. 2018, PASJ, 70, S8
- Alam, S., Ata, M., Bailey, S., et al. 2017, MNRAS, 470, 2617
- Albert, A., Anderson, B., Bechtol, K., et al. 2017, ApJ, 834, 110
- Bañados, E., Venemans, B. P., Mazzucchelli, C., et al. 2018, Nature, 553, 473
- Bechtol, K., Drlica-Wagner, A., Balbinot, E., et al. 2015, ApJ, 807, 50
- Becker, M. R., McKay, T. A., Koester, B., et al. 2007, ApJ, 669, 905
- Bell, E. F., Zucker, D. B., Belokurov, V., et al. 2008, ApJ, 680, 295
- Bernard, E. J., Ferguson, A. M. N., Schlafly, E. F., et al. 2016, MNRAS, 463, 1759
- Bernstein, G. M., Armstrong, R., Plazas, A. A., et al. 2017, PASP, 129, 074503
- Bertin, E. 2011, in Astronomical Society of the Pacific Conference Series, Vol. 442, Astronomical Data Analysis Software and Systems XX, ed. I. N. Evans, A. Accomazzi, D. J. Mink, & A. H. Rots, 435
- Blake, C., Brough, S., Colless, M., et al. 2011, MNRAS, 415, 2876
- Bohlin, R. C., Mészáros, S., Fleming, S. W., et al. 2017, AJ, 153, 234
- Burke, D. L., Rykoff, E. S., Allam, S., et al. 2018, AJ, 155, 41
- Burleigh, K., Dey, A., Lang, D., Schlegel, D. J., & DECaLS/MzLS/BASS Collaboration. 2018, AJ, 999, 999
- Carballo-Bello, J. A., Martínez-Delgado, D., Navarrete, C., et al. 2018, MNRAS, 474, 683
- Carlberg, R. G. 2009, ApJL, 705, L223
- Chambers, K. C., Magnier, E. A., Metcalfe, N., et al. 2016, ArXiv e-prints, arXiv:1612.05560
- Coupon, J., Broadhurst, T., & Umetsu, K. 2013, ApJ, 772, 65
- Coupon, J., Arnouts, S., van Waerbeke, L., et al. 2015, MNRAS, 449, 1352
- Cutri, R. M., Wright, E. L., Conrow, T., et al. 2012, Explanatory Supplement to the WISE All-Sky Data Release Products, Tech. rep.
- Dark Energy Survey Collaboration, Abbott, T., Abdalla, F. B., et al. 2016, MNRAS, 460, 1270
- Dawson, K. S., Kneib, J.-P., Percival, W. J., et al. 2016, AJ, 151, 44
- de Jong, J. T. A., Verdoes Kleijn, G. A., Boxhoorn, D. R., et al. 2015, A&A, 582, A62
- DESI Collaboration, Aghamousa, A., Aguilar, J., et al. 2016a, ArXiv e-prints, arXiv:1611.00036
- . 2016b, ArXiv e-prints, arXiv:1611.00037
- Dey, A., Rabinowitz, D., Karcher, A., et al. 2016, in Proc. SPIE, Vol. 9908, Ground-based and Airborne Instrumentation for Astronomy VI, 99082C
- Djorgovski, S. G., Mahabal, A., Drake, A., Graham, M., & Donalek, C. 2013, Sky Surveys, ed. T. D. Oswalt & H. E. Bond, 223
- Drlica-Wagner, A., Bechtol, K., Rykoff, E. S., et al. 2015, ApJ, 813, 109
- Eisenstein, D. J., Blanton, M., Zehavi, I., et al. 2005, ApJ, 619, 178
- Flaugher, B., Diehl, H. T., Honscheid, K., et al. 2015, AJ, 150, 150
- Gaia Collaboration, Brown, A. G. A., Vallenari, A., et al. 2016a, A&A, 595, A2
- Gaia Collaboration, Prusti, T., de Bruijne, J. H. J., et al. 2016b, A&A, 595, A1
- Grillmair, C. J. 2009, ApJ, 693, 1118
- Groom, D. 2004, in Astrophysics and Space Science Library, Vol. 300, Scientific Detectors for Astronomy, The Beginning of a New Era, ed. P. Amico, J. W. Beletic, & J. E. Beletic, 81–93
- Guzzo, L., Pierleoni, M., Meneux, B., et al. 2008, Nature, 451, 541
- Helmi, A., Cooper, A. P., White, S. D. M., et al. 2011, ApJL, 733, L7

- Hogg, D. W., Blanton, M. R., Eisenstein, D. J., et al. 2003, *ApJL*, 585, L5
- Hood, C. E., Kannappan, S. J., Stark, D. V., et al. 2018, *ArXiv e-prints*, arXiv:1803.05447
- Ivezić, Ž., Sesar, B., Jurić, M., et al. 2008, *ApJ*, 684, 287
- Jiang, T., Hogg, D. W., & Blanton, M. R. 2012, *ApJ*, 759, 140
- Jurić, M., Ivezić, Ž., Brooks, A., et al. 2008, *ApJ*, 673, 864
- Laevens, B. P. M., Martin, N. F., Sesar, B., et al. 2014, *ApJL*, 786, L3
- Lam, T. Y., Nishimichi, T., Schmidt, F., & Takada, M. 2012, *Physical Review Letters*, 109, 051301
- Lan, T.-W., Ménard, B., & Zhu, G. 2014, *ApJ*, 795, 31
- Lang, D. 2014, *AJ*, 147, 108
- Lang, D., Hogg, D. W., & Mykytyn, D. 2016a, The Tractor: Probabilistic astronomical source detection and measurement, *Astrophysics Source Code Library*, ascl:1604.008
- Lang, D., Hogg, D. W., & Schlegel, D. J. 2016b, *AJ*, 151, 36
- Li, T. S., DePoy, D. L., Marshall, J. L., et al. 2016, *AJ*, 151, 157
- Mainzer, A., Bauer, J., Cutri, R. M., et al. 2014, *ApJ*, 792, 30
- Mandelbaum, R., Wang, W., Zu, Y., et al. 2016, *MNRAS*, 457, 3200
- Masjedi, M., Hogg, D. W., Cool, R. J., et al. 2006, *ApJ*, 644, 54
- Meisner, A. M., Lang, D., & Schlegel, D. J. 2017a, *AJ*, 154, 161
- . 2017b, *AJ*, 153, 38
- . 2017c, *ArXiv e-prints*, arXiv:1710.02526
- . 2018, *Research Notes of the American Astronomical Society*, 2, 1
- Ménard, B., Scranton, R., Schmidt, S., et al. 2013, *ArXiv e-prints*, arXiv:1303.4722
- Myers, A. D., White, M., & Ball, N. M. 2009, *MNRAS*, 399, 2279
- Myers, A. D., Palanque-Delabrouille, N., Prakash, A., et al. 2015, *ApJS*, 221, 27
- Newberg, H. J., Yanny, B., Rockosi, C., et al. 2002, *ApJ*, 569, 245
- Newman, J. A. 2008, *ApJ*, 684, 88
- Odenkirchen, M., Grebel, E. K., Dehnen, W., et al. 2003, *AJ*, 126, 2385
- Oke, J. B., & Gunn, J. E. 1983, *ApJ*, 266, 713
- Padmanabhan, N., Schlegel, D. J., Finkbeiner, D. P., et al. 2008, *ApJ*, 674, 1217
- Pezzotta, A., de la Torre, S., Bel, J., et al. 2017, *A&A*, 604, A33
- Plazas, A. A., Bernstein, G. M., & Sheldon, E. S. 2014, *PASP*, 126, 750
- Prakash, A., Licquia, T. C., Newman, J. A., et al. 2016, *ApJS*, 224, 34
- Raichoor, A., Comparat, J., Delubac, T., et al. 2017, *MNRAS*, 471, 3955
- Reil, K., Lewis, P., Schindler, R., & Zhang, Z. 2014, in *Proc. SPIE*, Vol. 9149, *Observatory Operations: Strategies, Processes, and Systems V*, 91490U
- Ruhland, C., Bell, E. F., Rix, H.-W., & Xue, X.-X. 2011, *ApJ*, 731, 119
- Rykoff, E. S., Rozo, E., Busha, M. T., et al. 2014, *ApJ*, 785, 104
- Rykoff, E. S., Rozo, E., Hollowood, D., et al. 2016, *ApJS*, 224, 1
- Schlafly, E. F., Finkbeiner, D. P., Jurić, M., et al. 2012, *ApJ*, 756, 158
- Schlafly, E. F., Green, G. M., Lang, D., et al. 2018, *ApJS*, 234, 39
- Schmidt, S. J., Ménard, B., Scranton, R., Morrison, C., & McBride, C. K. 2013, *MNRAS*, 431, 3307
- Scott, D., Pierfederici, F., Swaters, R. A., Thomas, B., & Valdes, F. G. 2007, in *Astronomical Society of the Pacific Conference Series*, Vol. 376, *Astronomical Data Analysis Software and Systems XVI*, ed. R. A. Shaw, F. Hill, & D. J. Bell, 265
- Shanks, T., Metcalfe, N., Chehade, B., et al. 2015, *MNRAS*, 451, 4238
- Shipp, N., Drlica-Wagner, A., Balbinot, E., et al. 2018, *ArXiv e-prints*, arXiv:1801.03097
- Skrutskie, M. F., Cutri, R. M., Stiening, R., et al. 2006, *AJ*, 131, 1163
- Tal, T., van Dokkum, P. G., Franx, M., et al. 2013, *ApJ*, 769, 31
- The Dark Energy Survey Collaboration. 2005, *ArXiv Astrophysics e-prints*, astro-ph/0510346
- Valdes, F., Gruendl, R., & DES Project. 2014, in *Astronomical Society of the Pacific Conference Series*, Vol. 485, *Astronomical Data Analysis Software and Systems XXIII*, ed. N. Manset & P. Forshay, 379
- Watson, D. F., Berlind, A. A., & Zentner, A. R. 2012, *ApJ*, 754, 90

- Williams, G. G., Olszewski, E., Lesser, M. P., & Burge, J. H. 2004, in Society of Photo-Optical Instrumentation Engineers (SPIE) Conference Series, Vol. 5492, Ground-based Instrumentation for Astronomy, ed. A. F. M. Moorwood & M. Iye, 787–798
- Willman, B., Dalcanton, J. J., Martinez-Delgado, D., et al. 2005, *ApJL*, 626, L85
- Wright, E. L., Eisenhardt, P. R. M., Mainzer, A. K., et al. 2010, *AJ*, 140, 1868
- Yanny, B., Newberg, H. J., Grebel, E. K., et al. 2003, *ApJ*, 588, 824
- Yoon, J. H., Johnston, K. V., & Hogg, D. W. 2011, *ApJ*, 731, 58
- Zheng, Z., Zehavi, I., Eisenstein, D. J., Weinberg, D. H., & Jing, Y. P. 2009, *ApJ*, 707, 554
- Zhu, G., & Ménard, B. 2013, *ApJ*, 770, 130
- Zou, H., Zhou, X., Fan, X., et al. 2017a, *PASP*, 129, 064101
- Zou, H., Zhang, T., Zhou, Z., et al. 2017b, *AJ*, 153, 276
- . 2017c, ArXiv e-prints, arXiv:1712.09165
- Zu, Y., Weinberg, D. H., Jennings, E., Li, B., & Wyman, M. 2014, *MNRAS*, 445, 1885

Facility: KPNO:Mayall (Mosaic3)

Facility: Steward:Bok (90Prime)

Facility: CTIO:Blanco (DECam)

Facility: WISE

Facility: Gaia